Modelling residual stresses in sand-cast superduplex stainless steel

Numerical/experimental investigation about the residual stresses in the cooling phase of a sand casting process for superduplex stainless steel

G.Palumbo[1, a], A.Piccininni[1, b], V.Piglionico[1, c], P.Guglielmi[1, d], D.Sorgente[1, e] and L. Tricarico[1, f]

[1]DMMM – Politecnico di Bari, viale Japigia 182 – Bari, Italy

[a]g.palumbo@poliba.it, [b]antonio.piccininni@poliba.it, [c]vito.piglionico@poliba.it, [d]pasquale.guglielmi@poliba.it, [e]d.sorgente@poliba.it, [f]tricarico@poliba.it

Abstract

Residual stresses are a widespread phenomenon in manufacturing, since affecting all the processes characterised by heating and consequent cooling phase, like: machining, welding, casting or simply an heat treatment.

In particular, residual stresses usually negatively affect casted components, by changing the final shape (distortions) before or after the machining phase, by creating cracks which limit (or completely compromise) the performance in working conditions.

In the present work a numerical procedure based on the adoption of a Finite Element model is proposed for calculating the residual stress state during the cooling phase of a superduplex stainless steel (ASTM A890 Gr. 5A) casting. The numerical analysis has been strongly supported by a wide experimental activity aimed at: (i) determining the material characteristics in a large temperature range (from room temperature up to 1200°C) in terms of both mechanical characteristics (Young moduli and flow curves) and creep behaviour ; (ii) acquiring temperature data in different points of the casting during the cooling phase; (iii) validating numerical results in terms of displacements produced by residual stresses after cutting the component.

A fully coupled thermo-mechanical analysis was carried out neglecting the presence of the sand mould and setting heat transfer coefficients (through an inverse analysis) in order to fit temperature evolutions acquired during instrumented casting tests. On the contrary, much larger attention was paid to the material modelling: experimental data coming from tensile and creep tests were implemented in the model. In particular, residual stresses calculated by modelling the material behaviour simply in terms of flow stress curves were compared with the ones obtained by including also the creep behaviour in the FE model.

The final comparison with relaxation measurements after cutting the castings revealed that the numerical model implementing the creep behaviour is able to accurately predict experimental data, thus confirming that the presence of the viscous contribute during cooling noticeably affects the residual stress phenomenon in the casting process.

Keywords: *Superduplex Stainless Steels (ASTM A890 Gr. 5A), Finite Element Method, Residual Stresses, Casting, Creep Modelling.*

1. Introduction

Casting of metal alloys is largely adopted for manufacturing complex components; among the adopted methodologies, obviously the most common, flexible and able to produce big components, is the sand casting where melt metal is poured into a mould, usually composed of sand and a chemical binder. Often parts manufactured by this process are characterised by several defects; many of them can be related to the cooling phase and/or how the cast cools down. One of the most important phenomena to be investigated and predicted is the residual stress state since it negatively affects casted components by changing their final shape (distortions) before or after the machining phase and/or by creating cracks which limit (totally or partially) the performance in working conditions.

As reported by Totten et al. (2001), if different regions of the casting could cool at a uniform rate or alternatively a uniform constraint could act over the whole casting surface, room temperature would be reached without any distortion and any residual stress state; in real castings, the contraction of adjacent regions characterised by different cooling rates is the main reason why thermal stresses arises and, if they exceed the yield stress of the material, remain as a residual state of stress at room temperature, when the thermal equilibrium has been reached.

In spite of the above mentioned drawbacks, casting process remains the only solution for the production of large scale components, in particular for Oil and Gas applications, which needs components characterised by superior performances in terms of mechanical properties and corrosion resistance.

According to Mc Guire (2008), among the alloys suitable for the Oil and Gas industry, duplex alloys are considered one of the most interesting within the big family of stainless steels (SS), since they can match the abovementioned needs due

to their biphasic austenitic – ferritic microstructure. Such alloys reach the best performance when the two phases are equally partitioned within the structure (50-50%).

At the same time, this type of SS is characterized by the well-known drawback of the formation of embrittling secondary phases, responsible for dramatic reduction of both mechanical properties and corrosion resistance.

In order to predict the evolution of residual stresses with high level of accuracy, the numerical approach results to be the most reliable solution: building up an accurate simulating structure is the starting point to understand this phenomenon. From a theoretical point of view, the evolution of residual stress involves the solution of the thermal and the subsequent mechanical problem: in such a scenario, it is well known that finite difference method (FDM) is more efficient in the flow analysis while finite element method (FEM) is more accurate below the solidus temperature. In fact Si et al. (2003), as well as Liu et al. (2001), adopted a sort of hybrid method in which temperature history was obtained using a FDM solver and subsequently imported within the FEM environment in order to calculate the thermal strains. Lewis and Ravindran (2000), in addition, paid great attention to the modelling of the melting/solidification transformation accompanied by the release/absorption of latent heat at the liquid/solid interface.

An alternative procedure is the more conventional fully coupled thermo-mechanical analysis, which is mainly based on the simultaneous solution of the two sets of equations governing the problem: Fackeldey et al. (2000) proposed a numerical model which, starting from the filling phase, is able to predict not only the temperature distribution and the stress evolution, but also the dendritic

structure as well as the amount of eutectic fraction thanks to the implementation of an accurate microstructural model.

The accuracy of the numerical prediction is not only a matter of the solution methodology, but it also depends on the correct modelling of both the sand and the alloy properties: Baghani et al. (2014) discussed the influence of the sand stiffness demonstrating that if the mould is modelled as a rigid body, it determines an overestimation of the stresses at the end of cooling; the author thus inferred that an elasto-plastic mechanical behaviour can be considered as the most accurate formulation for modelling the sand. The same results were reached by Motoyama et al. (2013) and by Inoue et al. (2013): good accordance between numerical and experimental results (in terms of: restraint force applied by the sand, casting contraction , temperature evolution) could be obtained when adopting the elasto – plastic model, while a fully elastic behaviour led to value of the maximum numerical applied restraint force four time larger than the one experimentally determined.

The approach of modelling the sand mould and its properties determine quite large computing times, most of all related to the sand mesh and the interaction between the casting and the mould. However the largest quantity of the element nodes belongs to the mould; so, replacing the mould with equivalent boundary conditions, should be an attractive solution in order to both simplify the model creation and reduce the simulation time. In fact, Metzeger et al. (2001), as well as Chang and Dantzig (2004), proposed a surface element formulation able to replace the sand mould action in stress determination by applying appropriate normal forces to the casting surface: in particular, the proposed element was designed as a

four nodes quadrilateral element positioned on the exposed surface of eight-node three dimensional hexahedral elements composing the casting mesh.

However, as confirmed by literature, the correct choice for the mechanical model able to describe the alloy behaviour plays a key role in the simulation of this phenomenon: in particular, considering the wide range of temperatures the material is subjected to during the cooling phase and the high strain rate sensitivity at elevated temperature, a fully elastic (or elasto-plastic) behaviour may lead to inaccurate results. As confirmed by the work of Fachinotti and Cardona (2003), who presented a list of constitutive equations to be applied for modelling the steel behaviour at high temperature, rate dependent viscoplasticity resulted to be the most accurate formulation, even if it is more time consuming than a conventional plastic model; Vila Real et al. (2004) proposed a thermo-elasto-viscoplastic behaviour based on the constitutive equation of Perzyna, obtaining good accordance between numerical and experimental results; Koric and Thomas (2008) performed a double parallel approach considering two different elasto – viscoplastic constitutive laws (Kozlowski in combination with the Zhu power law and the Anand law for steel) respectively applied on two models build on two different commercial finite element solvers (ABAQUS and ANSYS): both of the two model revealed to be quite precise in predicting residual stresses, but the Kozlowski/Zhu model was more accurate when compared with experimental results.

Being the aim to have an efficient and fast numerical tool able to predict the state of stress of a sand casting at room temperature, in this work a different approach for the evaluation of the residual stress state after the cooling phase of a sand casting process was used, as detailed in the section 2.1.

2. Material & Methods

2.1 Methodology

The growth of the residual stress depends, above all of the factors, on the differences of the cooling rates in different zones of the casting geometry; with this concept in mind, the design of a part similar to the one adopted by Gustafsson et al. (2009) in their work was used, since from the analysis of the literature it appears able to emphasize the above mentioned difference in terms of cooling rates. In this study, the proposed geometry consists of three parallel bars characterized by different cross sections, whose contraction during cooling is constrained by two massive regions (yokes) at both of the ends of the bars. In particular, the central bar has a cross section larger than the side bars: the difference in the cross sections consequently determines a difference in the Chvorinov ratio of volume to surface area (or cooling modulus) which is well known to be related to the cooling rate (Figure 1).

Main quotes of the proposed benchmark geometry are reported in Table1; in order to understand how the difference of cooling moduli between central and side bars could affect the evolution of residual stresses, an alternative geometry was also designed (Geometry B), characterised by the value of the cross section area of each side bar similar to the one of the central bar.

Since temperature evolution plays an important role during such a phenomenon, at first great attention was paid to the solution of the thermal problem, that was differently solved from what is usually reported in literature: sand mould was no longer modelled and the heat exchange was totally managed by the convection laws. An inverse analysis was thus necessary in order to determine the heat transfer coefficients between the casting and the sand mould (as a function of the

temperature) able to minimize the difference between the numerical temperature evolutions and the acquisitions by instrumented casting experiments.

A great attention was paid to the material modelling, carrying out experimental tests on the investigated alloy (tensile and creep tests): flow stress curves, elastic moduli and also the creep behaviour were thus implemented in the FE model.

In order to understand if the adopted approach was robust and reliable, the numerical model was also validated: in particular, wire cuts by electro discharge machining were carried out on the casting so that the relaxation after the stress redistribution could be used as an indicator of the residual stress entity; the same procedure was numerically modelled and results were compared.

As a confirmation of the robustness of the proposed methodology, the same procedure was finally replicated using the Geometry B.

2.2 Tensile and Creep Tests

In order to characterize the investigated alloy (ASTM A890 Gr. 5A, chemical composition in Table 2), a wide experimental activity, essentially based on tensile and creep tests, was carried out covering a wide range of temperatures, from room temperature up to 1200°C.

Both tensile and creep tests were carried out adopting the Gleeble System 3180 physical simulator: specimens were heated by Joule effect managing a PID controller in order to reach and maintain the target temperature by means of a thermocouple welded in the middle of the cylindrical specimen. In addition, because of the elevated temperature, tests were carried out under high vacuum conditions in order to limit the material oxidation.

The two geometries shown in Figure 2a and Figure2b were respectively used for tensile and creep tests.

2.3 Casting experiments

Resin patterns made by Selective Laser Sintering (SLS) technique were used for the sand molds creation; one of the two halves of the resin pattern was drilled in order to create the holes for positioning the thermocouples (Figure 3). Temperature data were acquired using B-type and K-type thermocouples, since both the casting and the mould were monitored; in particular, B-type thermocouples were positioned at the casting middle plane, while the K-type thermocouples were placed within the sand, 10 mm over the outer surface of the pattern. After the completion of the sand compacting phase (on a vibrational table), the thermocouples were wired and subsequently connected to the acquisition system (Figure 4): temperature data were acquired during the cooling phase (until the shake out) with a frequency of 2 Hz.

2.4 Numerical model

The FE model used for the numerical analyses was created in the ABAQUS CAE (v. 6.12) environment.

A total number of 12042 elements (C3D8T type, 8 node trilinear element with temperature degree of freedom) was used, refining the mesh in the fillet radius regions. As shown in Figure 5a, only half of the case study described in the section 2.1 was modelled. Because of the symmetry of both the geometry and the boundary conditions, a large reduction of computational costs was thus obtained. In addition, such and assumption, revealed to be useful also for the simulation of

the stress relaxation due to cuts. In fact, if removing the symmetry boundary conditions of the side bars, they can relax under the effect of the stress state. It was thus necessary to set additional constraints (points A and B in Figure 5b) in order to avoid numerical problems when simulating the wire cutting.

Real dimensions of the castings were used for the modelling, also including fillet radii of the bars; fillets of the yokes were on the contrary not considered since expected to have a negligible influence on the residual stress evolution.

The strain the material experiences during the cooling can be described by Eq.1:

$$\varepsilon_{tot} = \varepsilon_{el} + \varepsilon_{pl} + \varepsilon_{th} + \varepsilon_{cr} \quad (1)$$

where ε_{el} is the elastic strain, ε_{pl} is the plastic strain, ε_{th} is the thermal strain and ε_{cr} is the creep strain. The creep strain component was modelled according to the Bailey – Norton law in Eq.2, also known as the power law creep:

$$\dot{\varepsilon}^{cr} = A\sigma^{n}t^{m} \quad (2)$$

Such a formulation, in its time hardening form, includes the uniaxial equivalent deviatoric stress (σ) the total time (t) and time exponent (m) necessary to take into account the contribution of the primary creep stage.

The mechanical behaviour of the material was thus modelled using data from the experimental activity (elastic-viscoplastic characteristics, as a function of the temperature, were implemented).

The numerical evaluation of the residual stress was carried out adopting a fully coupled thermo–mechanical approach: the temperatures are integrated using a

backward-difference scheme and the nonlinear coupled system is solved using Newton's method. The exact implementation of Newton's method involves a non-symmetric Jacobian matrix as is illustrated in the following matrix representation of the coupled equations:

$$\begin{bmatrix} K_{uu} & K_{u\theta} \\ K_{\theta u} & K_{\theta\theta} \end{bmatrix} \begin{Bmatrix} \Delta u \\ \Delta\theta \end{Bmatrix} = \begin{Bmatrix} R_u \\ R_\theta \end{Bmatrix}$$

where Δu and $\Delta\theta$ are the respective corrections to the incremental displacement and temperature, K_{ij} are submatrices of the fully coupled Jacobian matrix, R_u and R_θ are the mechanical and thermal residual vectors, respectively.

The cooling phase was ideally divided into two steps: in the first one the cooling before the shake out (BSO step) is simulated; in the second one, after the shake out (ASO step), the cooling of the casting in air is simulated.

The BSO step time was set to 4800s (which is the time at which the shake out procedure was performed during casting experiments), while the ASO step time was set to 20000 s (which is the time the casting needed to reach the room temperature).

3. Results and Discussion

3.1 Material characterization and modelling

Results of tensile tests have been resumed in Figure 6a; in the part b of the same figure strain curves from creep tests at 800°C have been plotted (up to the secondary stage). As concerns the flow stress curves, it may be noted that, as the temperature was increased, the material hardening became less evident; above the

temperature of 600°C the alloy behaviour can be considered fully plastic. As concerns the creep curves (Figure 6b), results at the temperature of 800°C prove that, despite the stress applied was lower than the correspondent yield stress, a not negligible strain after 800s affected the specimen, thus demonstrating that viscous behaviour plays a key role especially at temperatures higher than 600°C.

Data coming from the creep tests were analysed so that they could be implemented within the FE model: as shown in Figure 7, the values of the inelastic strain rate ($\dot{\varepsilon}_{in}$) coupled with the correspondent value of the applied stress (σ) where plotted on a double-log graph at three different levels of temperature (600, 800 and 1000°C).

For each level of the investigated temperatures, data were fitted using a first order equation whose slope and intercept represent respectively the stress order (n) and the power law multiplier (A) to be implemented (Eq.2) in the FE model (since results from creep tests showed a predominance of the secondary creep stage, when the strain rate can be assumed to be constant, the time exponent was set equal to 0).

3.2 Temperature acquisition during cooling and stress relaxation measurements

Temperature data, acquired from the casting experiments in the labs of the CSM (Rome) using both the geometries, have been plotted in Figure 8 limiting the attention to the middle points of the bars (central and lateral one).

The analysis of Figure 8 clearly shows the effect of the cooling modulus on the time evolution of temperature.

For each casting geometry, three replications were performed: as example, curves coming from the B1 thermocouple (positioned within one of the two yokes) have been plotted in Figure 9: data resulted to be highly repeatable since the curves are almost perfectly overlapped.

Experimental estimation of the residual stress state was carried out using a stress-relaxation technique, which is widely used in casting processes (aluminium, carbon and stainless steels) even if it is included in the group of the destructive techniques by Rossini et al. (2012). In such a technique the casting is subjected to cuts and the subsequent relaxation is the consequence of the residual stress redistribution.

As shown in Figure 10, in this work, the above mentioned technique was adopted performing Electro Discharge Machining (EDM) wire cut on both of the two side bars.

Before cutting the side bars, a physical reference mark was created on the right yoke (see Figure 10a) in order to use it for referring the wire positioning. Once the cut was completed and consequently the bars relaxed, the same machine was used for measuring the bar displacement by putting the wire in contact with the bar and referring its position to the reference mark: the actual position of the wire was compared with the one the wire had before the cut, thus obtaining the value of the relaxation in the longitudinal direction.

In the case of the Geometry A, both of the two bars relaxed of a quantity equal to 0.065±1E-4 mm; this results was further confirmed using a Coordinate Measurement Machine (0.065±4E-6 mm).

3.3 Numerical Analysis

A preliminary thermal analysis (focusing the attention on the BSO step) aimed at approximating the experimental temperature was needed. Differently from the conventional procedures reported in literature, only the casting geometry was modelled while the "thermal" action of the sand mould was taken into account through the presence of a surrounding environment (sink) whose temperature law was implemented according to the experimental acquisitions: such an approach led to consider the convection as the only phenomenon responsible for the heat transfer between the casting and the surrounding environment, thus dramatically reducing computational costs.

Also for this analysis the same model mesh shown in Figure 5 was adopted: the thermal symmetry was modelled applying a negligible heat flux in the symmetry region.

In order to make the results of this inverse analysis more accurate and considering that the heat transfer coefficients are influenced by several parameters such as the geometry of the exchanging bodies, the casting exchange surface was divided in the two groups shown in Figure 11a: the first one (Group#1) containing the side bars and the second one (Group#2 containing the central bar and both of the yokes.

In order to optimally fit experimental temperature evolutions, the heat transfer coefficients (changing according to the temperature) were set differently according to the specific region. Obtained results in terms of temperature evolutions have been shown in Figure 11b, highlighting a good fitting between experimental and numerical results. In addition, the HTC values concerning the

side bars as a function of the temperature have been compared with the HTC of the central bar and the yokes, as listed in Table 3.

Simulations results were analysed in terms of stress-time curves: the principal stress components (maximum and minimum, respectively SMax and SMin in the graphs) and the longitudinal stress (red curve) on the middle point of both the central bar and one of the side bar were monitored. The evolutions of the above mentioned stress components have been plotted in Figure 12 (not modelling the creep behaviour) and in Figure 13 (considering also the material viscous behaviour).

Stress evolutions clearly show that both the two bars are always characterised by an uniaxial state of stress: the maximum principal stress in the thinner bar (Figure 12a) is negligible at the end of the cooling phase, thus demonstrating that the side bar was subjected to a compressive residual state of stress; the opposite happens in the central bar, where the minimum principal stress can be considered negligible (Figure 12c).

Stress evolutions in Figure 13 were obtained by the model implementing the alloy viscous behaviour.

It is possible to note that the creep modelling has no influence on the type of the final stress state (once again uniaxial on both of the two bars). At the same time, as reported in Figure 14, the value of the predicted stress at room temperature are noticeably affected by the creep modelling (EVP label stands for “Elasto-Viscoplastic”, EP label stands for “Elasto-Plastic”).

3.4 Comparison and validation of the numerical model

Since the measurement of the residual state of stress can be inferred cutting the side bars, the same procedure was modelled by sequentially removing (in two separate static steps) the constraints on symmetry regions of the two side bars. Results in terms of displacements due to stress relaxation could be thus calculated in order to be compared with the experimental ones. In particular, the displacement due to stress relaxation was evaluated as shown in Figure 15: the distance between two fixed nodes (#1 e #2) was compared before (L_{bc})and after (L_{ac}) the constraint removal.

Numerical relaxations, both considering and neglecting the creep behaviour, were compared with the experimental results (as reported in Table 4). It may be noted that a good match between experimental and numerical data can be obtained when the creep behaviour is modelled; neglecting the viscous strain leads to an overestimation (more than twice) of the bar relaxation, of course due the overestimation of the residual stress state.

In order to confirm the robustness of the proposed analysis, the same procedure was applied also on the second designed geometry (Geometry B in Table 1). Numerical simulations were also in this case run both considering and neglecting the creep behaviour of the alloy; the wire cuts were simulated using the same approach and results in terms of displacements due to stress relaxation have been compared with the experimental ones. Results in terms of displacements measured on the part after removing the symmetry constraints on the two side bars are listed in Table 4.

According to experimental measurements, which demonstrated that negligible residual stresses were present at the end of cooling phase; the numerical

simulation implementing the material creep behaviour predicted a negligible value of the displacement due to relaxation (0.017mm). If only the plastic behaviour is modelled, the error increases up to 190%.

4. Conclusions

Residual stress state in casting is one of the major source of concern since it can change the final shape (distortions) of the component before or after the machining phase and can affect negatively its performance. A possible solution in order to predict the residual stress with high level of accuracy is the numerical simulation, once the material modelling has been properly set.

In this work, differently from the approaches reported in literature and from what commercial codes for casting simulations can actually perform, a novel methodology to numerically evaluate the residual stresses is presented: the absence of the sand mould modelling, the consequent heat exchange managed by the only convection laws and the refinement in material modelling relying on a elasto-viscoplastic behaviour are the key points of the proposed procedure.

Main results are resumed in the following list:

1. The thermal field was accurately simulated setting the values of the heat transfer coefficient (as function of the temperature) by means of an inverse analysis which allowed to minimize the difference between the numerical and experimental temperature evolutions.
2. The creep behaviour of the alloy shows to be the most influencing factor, since determining a large difference in the residual stress level (at room

temperature it was equal to half of the one determined if a simple elasto-plastic behaviour of the same alloy was considered).

3. As a consequence, a very good match (difference about 4 μm) between the experimental measurements of the casting relaxation after wire cutting and the correspondent numerical results could be obtained only taking into account the creep behaviour of the alloy.

4. The discrepancy in stresses evolution between the elasto – plastic and the elasto – viscoplastic model of course strongly affects the value of the numerical prediction of side bars relaxation (numerical results not considering viscous behaviour resulted to be twice greater than those coming from the approach modelling the material creep behaviour).

5. The proposed methodology appears to be robust since, applying the same procedure on a different casting geometry (in this case characterised by small differences of cooling rates between adjacent regions), gave again a good match between numerical results and experimental measurements after wire cutting.

Acknowledgments

The activities in this work were funded by the Italian Government in the framework of the European National Operative Programme for Research and Competitiveness (project acronym: SMATI).

References

Baghani, A., Davami, P., Varahram, N., Shabani, M.O., 2014. Investigation on the effect of mold constraints and cooling rate on residual stress during the sand-casting

process of 1086 steel by employing a thermo – mechanical model. Metall. Mater. Trans. B 45, 1157-1169.

Chang, A., Dantzig, J., 2004. Improved sand surface element for residual stress determination. Appl. Math. Model 28, 533-546.

Fachinotti, V.D., Cardona, A., 2003. Constitutive models of steel under continuous casting conditions. J. Mater. Process. Tech. 135, 30-43.

Fackeldey, M., Ludwig, A., Sahm, P.R., 1996. Coupled modelling of the solidification process predicting temperature, stresses and microstructures. Comp. Mater. Sci. 7, 194-199.

Gustafsson, E., Hofwing, M., Strömberg, N., 2009. Residual Stresses in a stress lattice – Experiments and finite element simulations. J. Mater. Process. Tech. 209, pp. 4320-4328.

Inoue, Y., Motoyama, Y., Takahashi, H., Shinji, K., Yoshida, M., 2013. Effect of sand mold models on the simulated mould restraint force and the contraction of the casting during cooling in green sand molds. J. Mater. Process. Tech. 213, 1157-1165.

Koric, S., Thomas, B.G., 2008. Thermo-mechanical models of steel solidification based on two elastic visco-plastic constitutive laws. J. Mater. Process. Tech 197, 408-418.

Lewis, R.W., Ravindran, K., 2000. Finite element simulation of metal casting. Int. J. Numer. Meth. Eng. 2, 29-59.

Liu, B.C., Kang, J.W., Xiong, S.M., 2001. A study on the numerical simulation of thermal stress during the solidification of shaped castings. Sci. Technol. Adv. Mater 2, 157-164.

Mc Guire, M.F., 2008. Stainless Steel for Designer Engineering. ASM International, 91-107.

Metzeger, D., Jarret New, K., Dantzig, J., 2001. A sand surface element for the efficient modelling of residual stress in castings. Appl. Math. Model. 25, 825-842.

Motoyama, Y., Inoue, Y., Saito, G., Yoshida, M., 2013. A verification of the thermal stress analysis including the furan sand mold, used to predict the thermal stress in castings. J. Mater. Process. Tech. 213, 2270-2277.

Rossini, N.S., Dassisti, M., Benyounis, K.Y., Olabi, A.G., 2012. Methods of measuring residual stresses in components. Mater. Design 35, 572-588.

Si, H.M., Cho, C., Kwakh, S.Y., 2003. A hybrid method for casting process simulation by combining FDM and FEM with an efficient data conversion algorithm. J. Mater. Process. Tech. 133, 311-321.

Totten, G., Howes, M., Inoue, T., 2002. Handbook of residual stresses and deformation of steel. ASM International, 361-371.

Vila Real, P.M.M., Oliveira, C.A.M., Barbosa, J.T., 2004. Thermo-elasto-viscoplastic numerical model for metal casting process. Int. J. Mech. Sci. 46, 245-261.

List of Figure captions

Figure 13 Residual stress state considering creep behaviour: a) Maximum and minimum principal stress on thinner bar, b) longitudinal stress on thinner bar, c) maximum and minimum principal stress on thinner bar, d) longitudinal stress on thicker bar.

Figure 14. Comparison between results from the models (implementing or not the creep behaviour): a) Side Bar, b) Central Bar

Figure 15. Scheme of determination of the side bar numerical relaxation

List of Table captions

Figure 1.

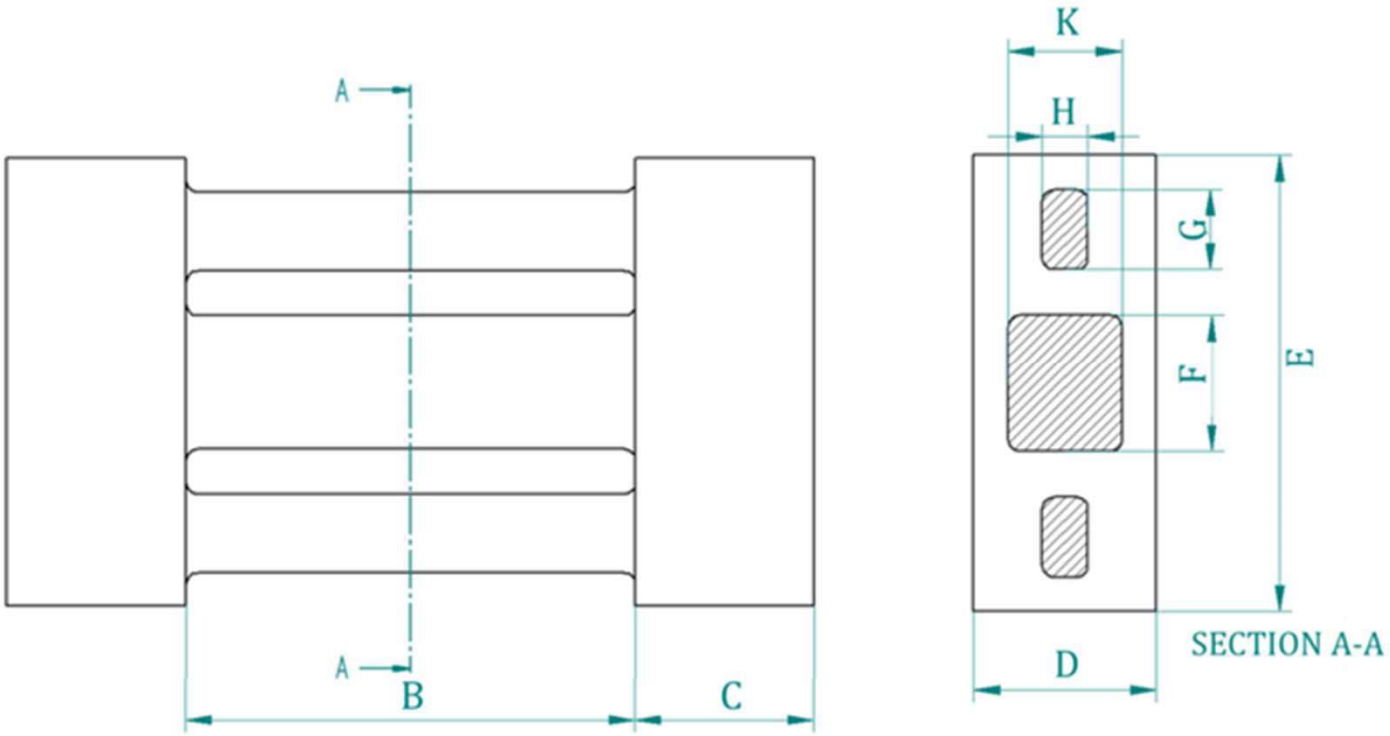

Figure 2a.

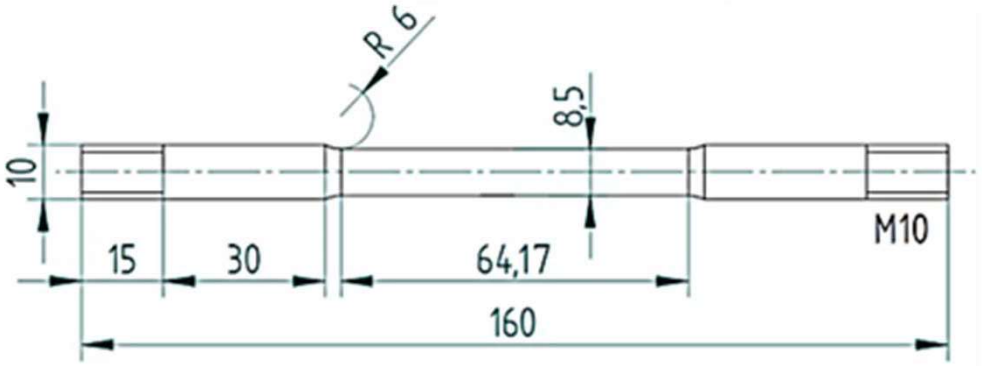

Figure 2b.

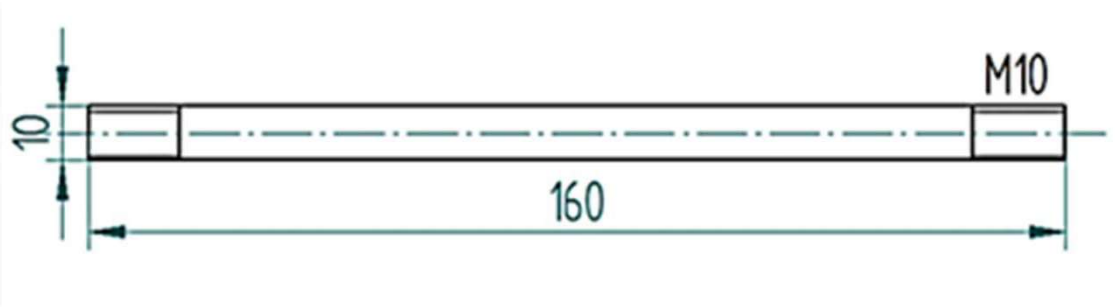

Figure 3.

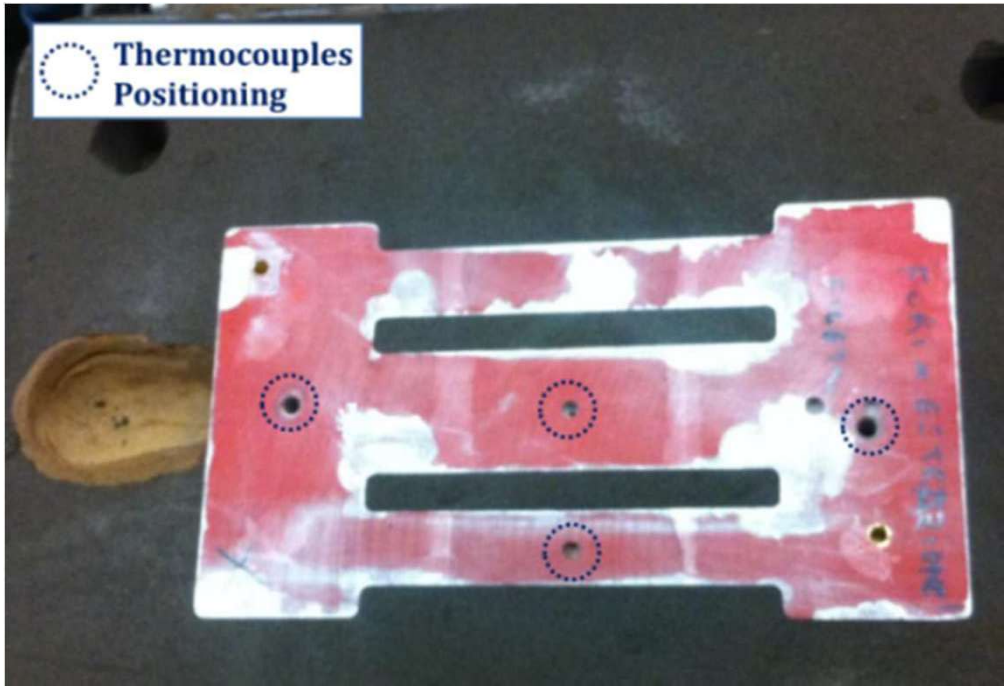

Figure 4.

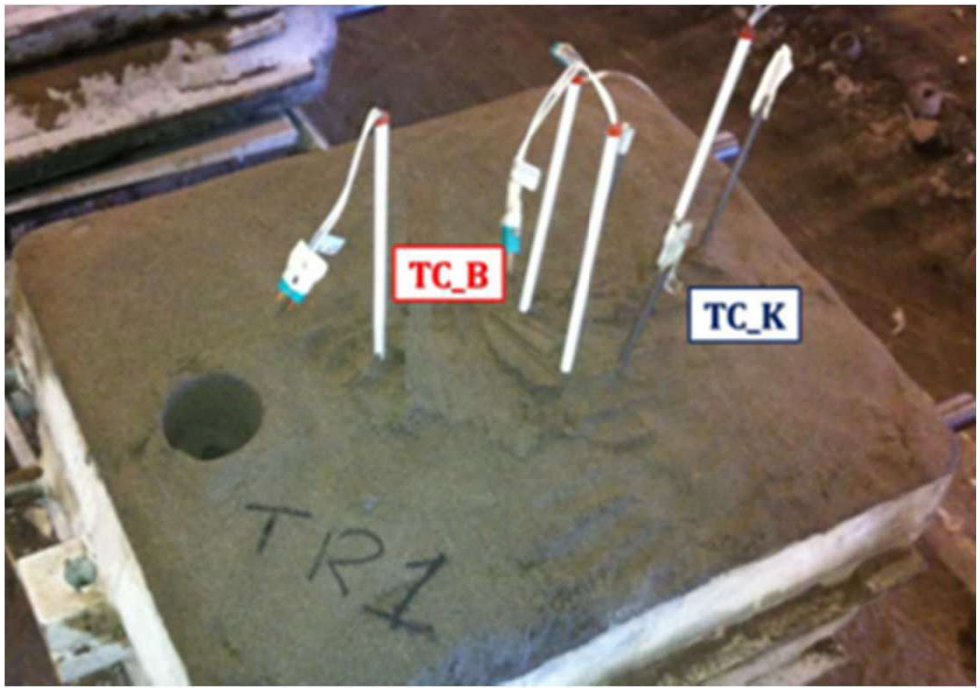

Figure 5a.

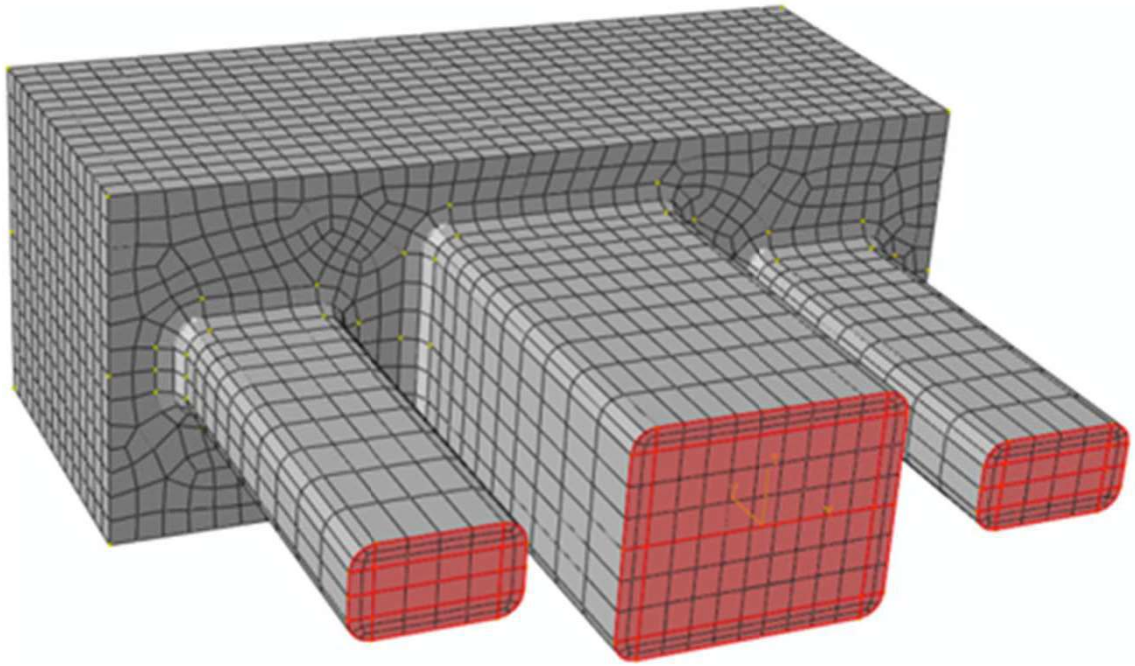

Figure 5b.

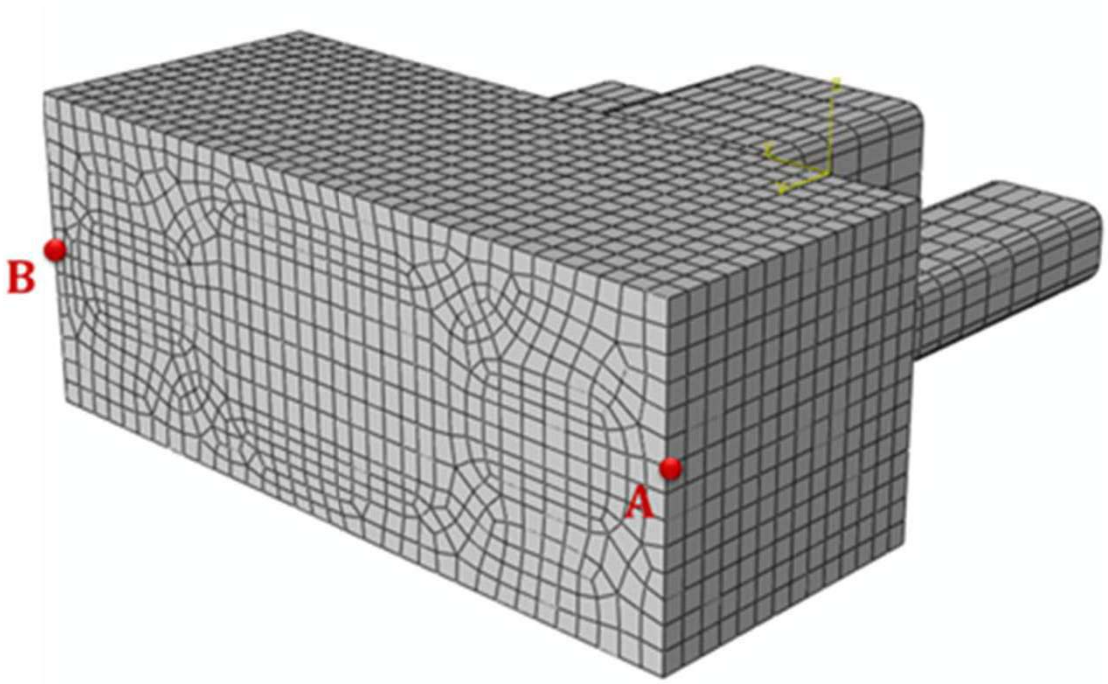

Figure 6a

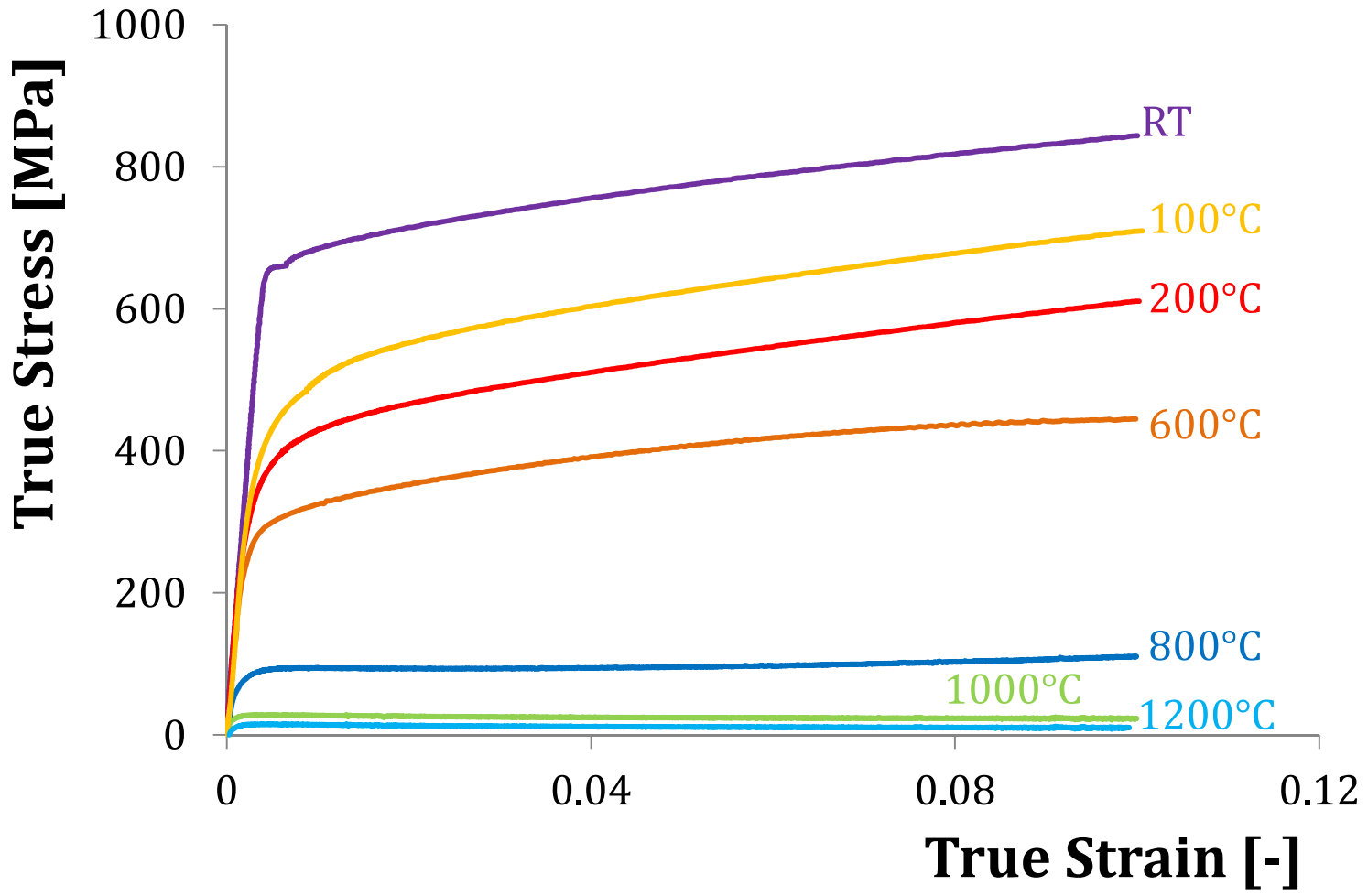
True Stress [MPa]
1000
800
600
400
200
0
0
0.04
0.08
0.12
True Strain [-]
RT
100°C
200°C
600°C
800°C
1000°C
1200°C

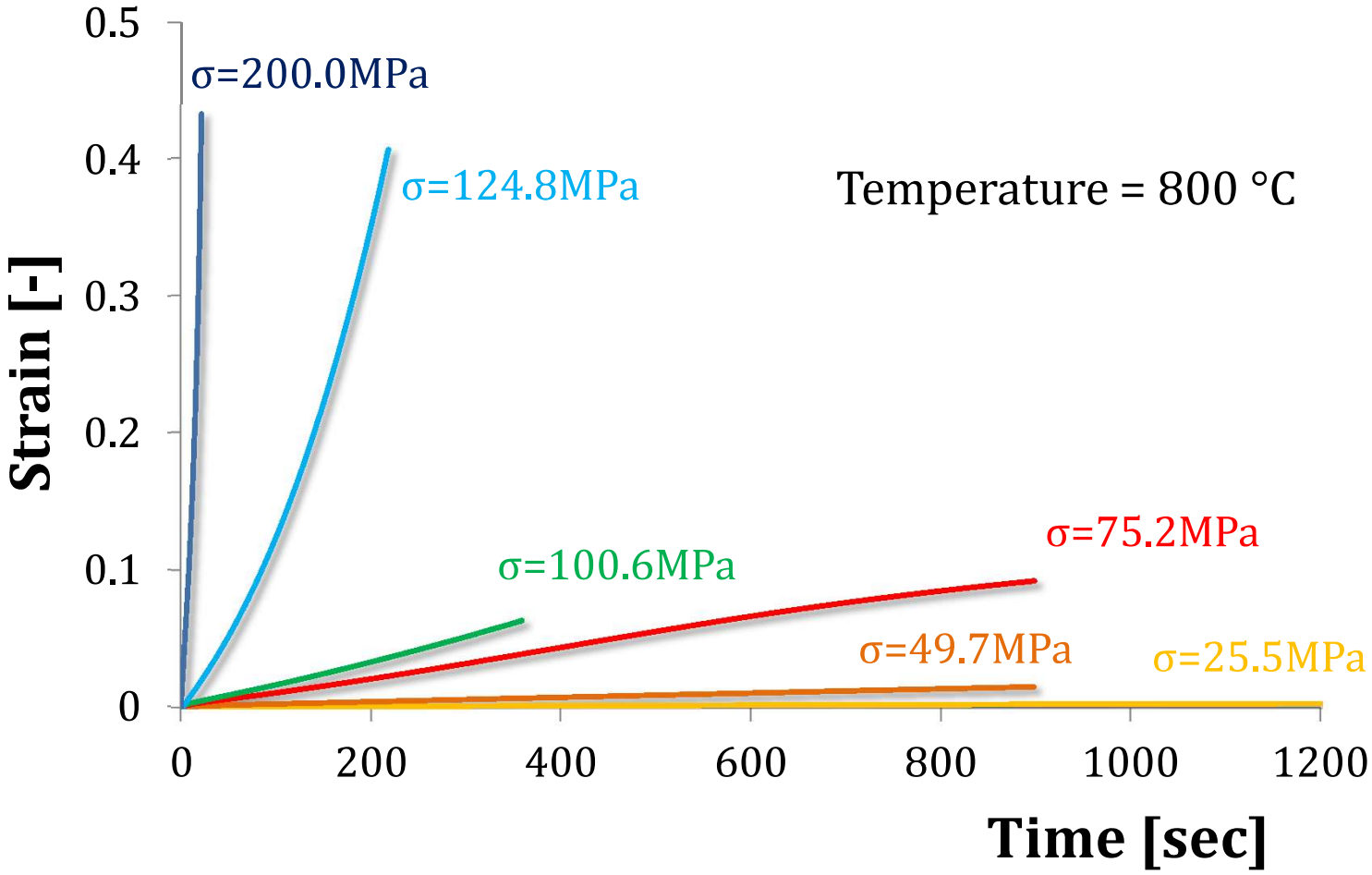
0.5
0.4
0.3
0.2
0.1
0
Strain [-]
σ=200.0MPa
σ=124.8MPa
Temperature = 800 °C
σ=75.2MPa
σ=100.6MPa
σ=49.7MPa
σ=25.5MPa
0
200
400
600
800
1000
1200
Time [sec]

Figure 6b

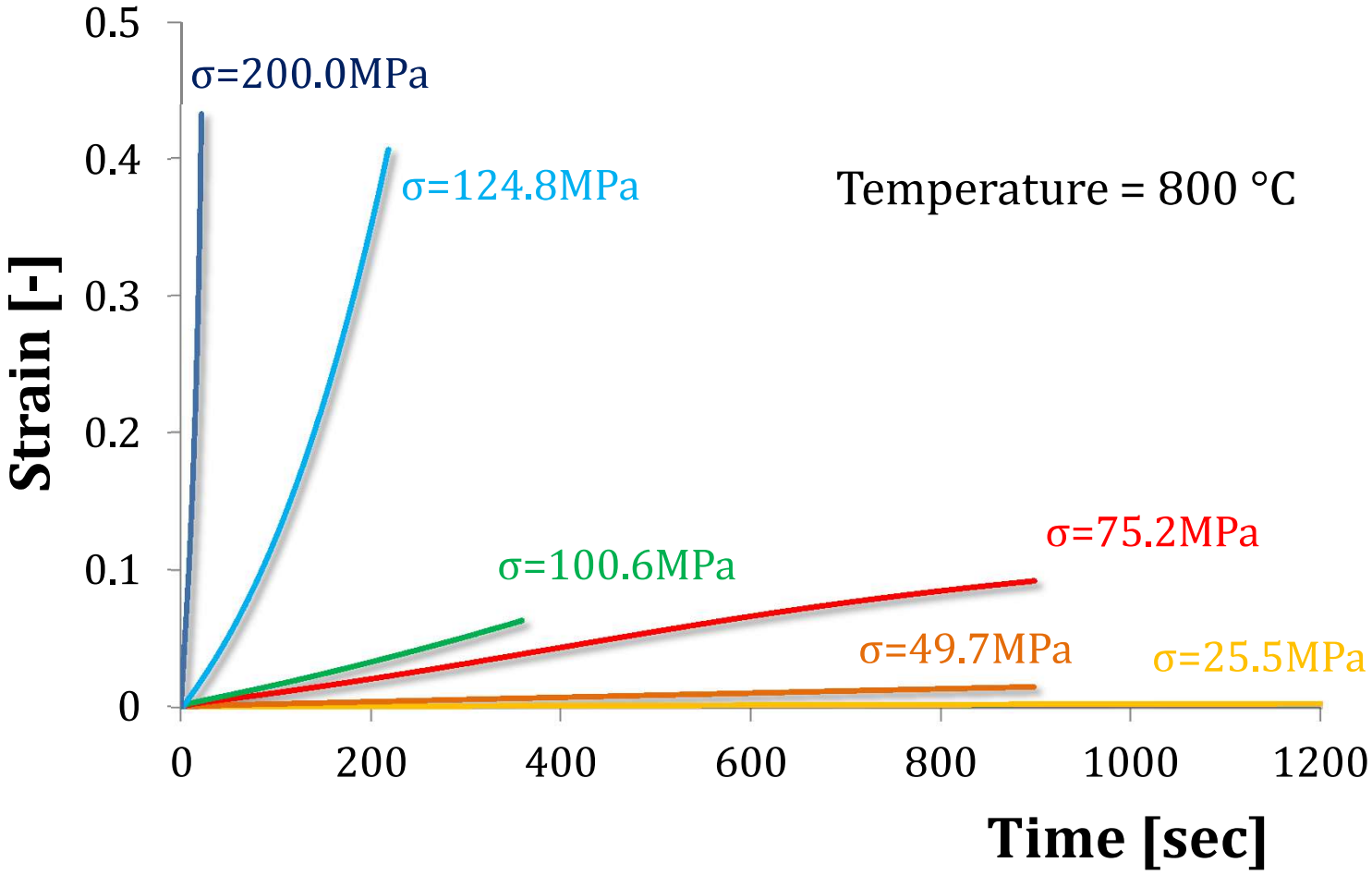
0.5
0.4
0.3
0.2
0.1
0
Strain [-]
σ=200.0MPa
σ=124.8MPa
Temperature = 800 °C
σ=75.2MPa
σ=100.6MPa
σ=49.7MPa
σ=25.5MPa
0
200
400
600
800
1000
1200
Time [sec]

Figure 7

Fig. 7

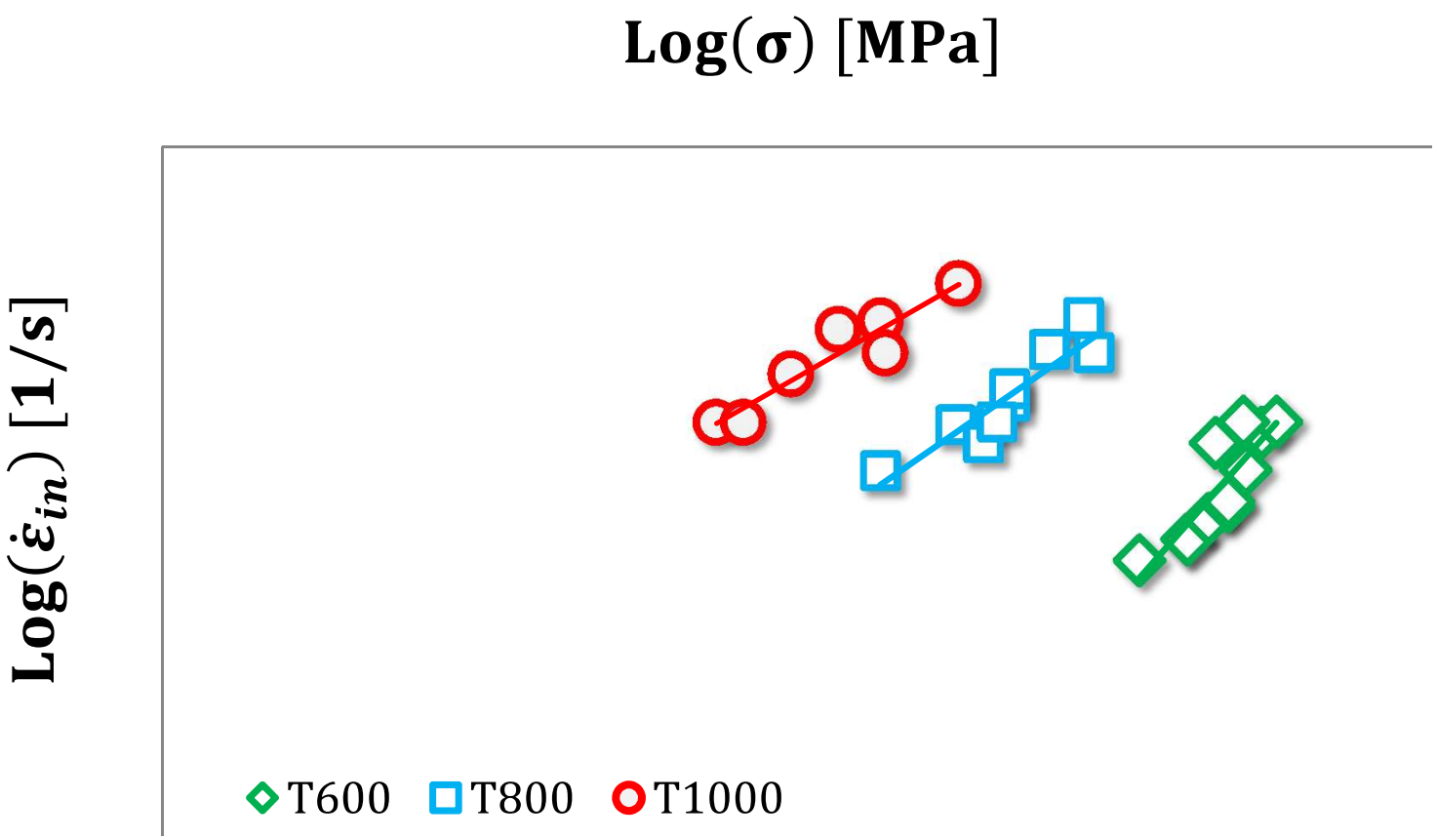

Figure 8a

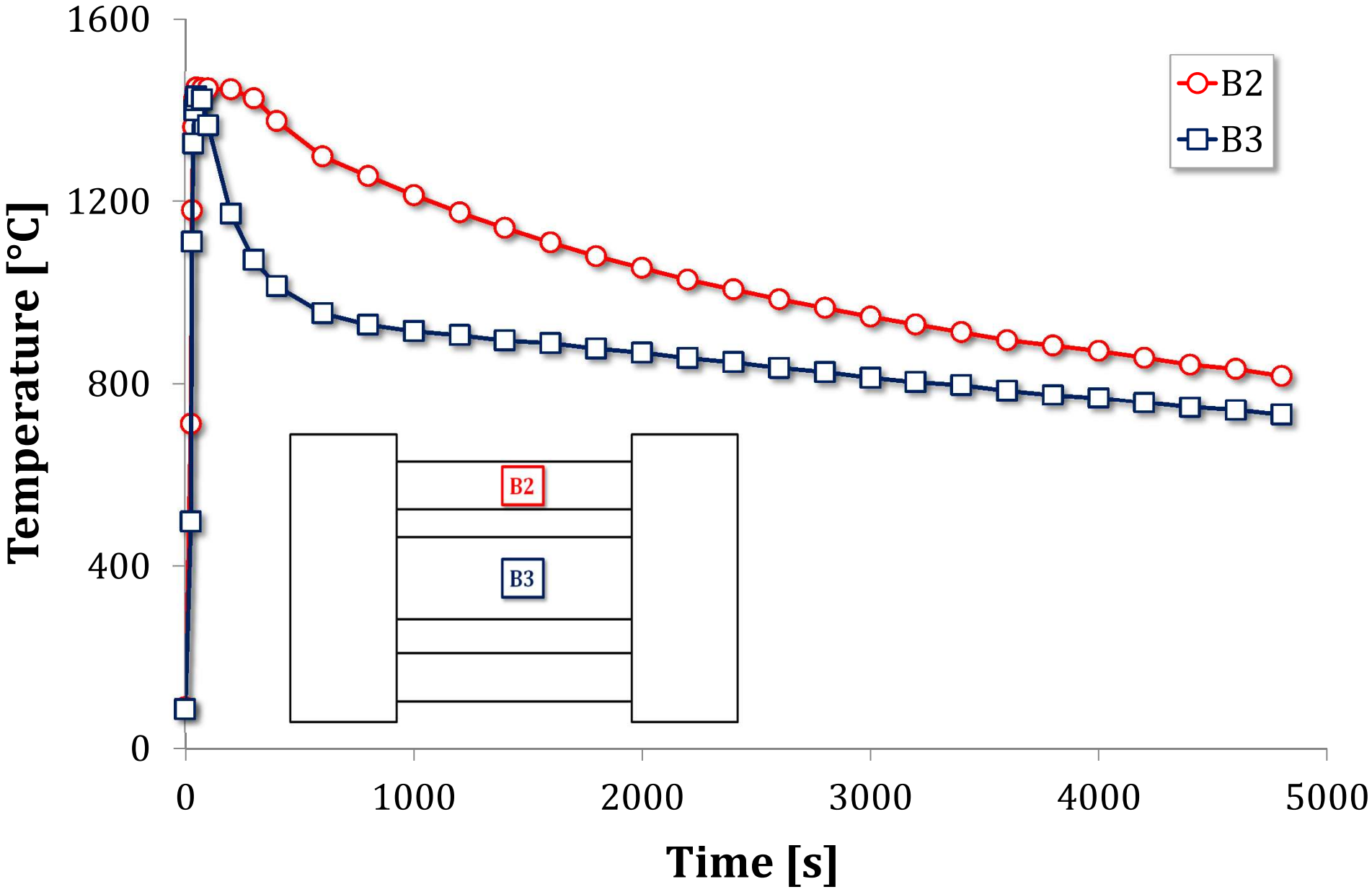
1600
1200
800
400
0
Temperature [°C]
0
1000
2000
3000
4000
5000
Time [s]
B2
B3
B2
B3

Figure 8b

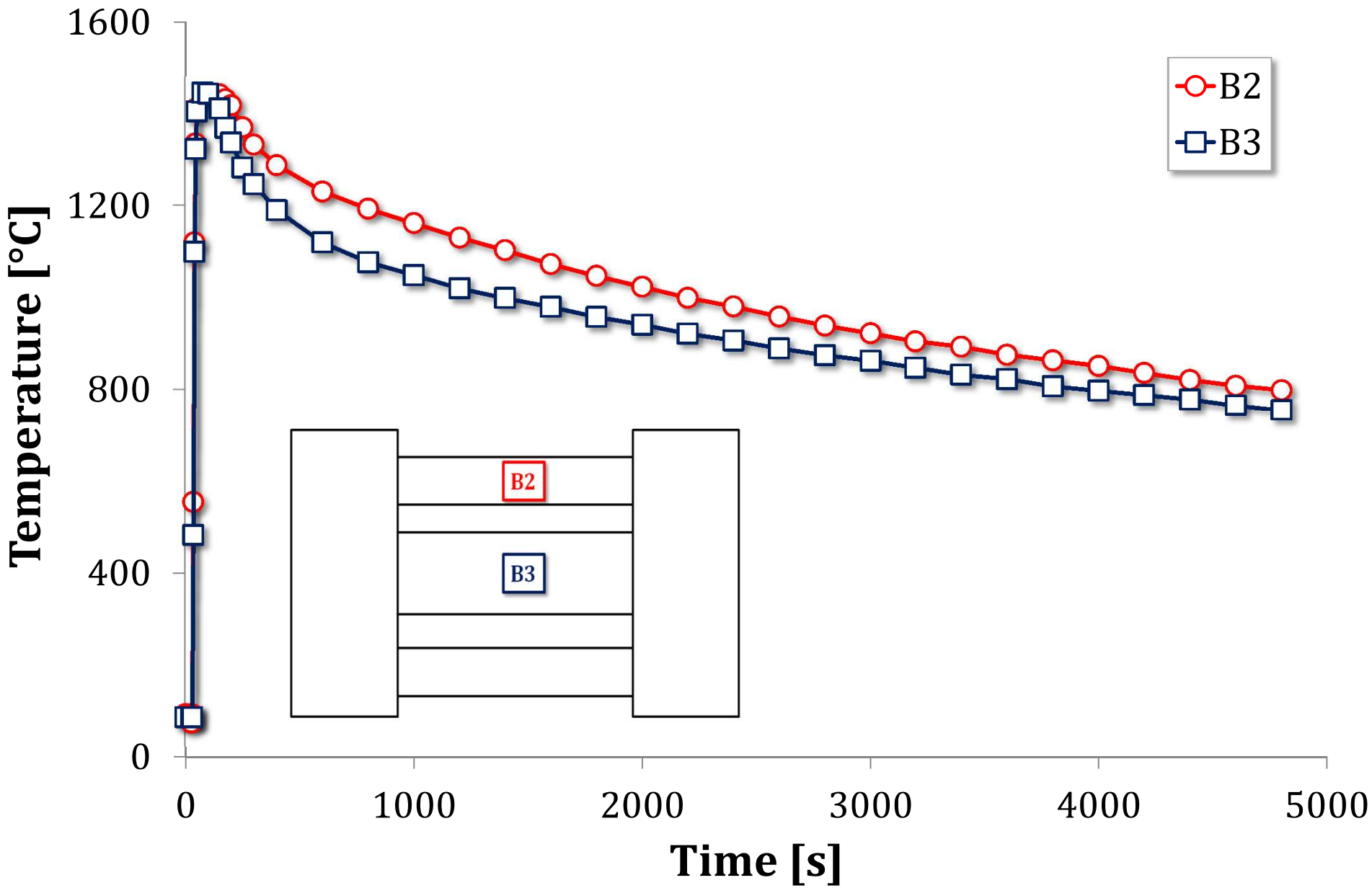
1600
1200
800
400
0
Temperature [°C]
0
1000
2000
3000
4000
5000
Time [s]
B2
B3
B2
B3

Figure 9

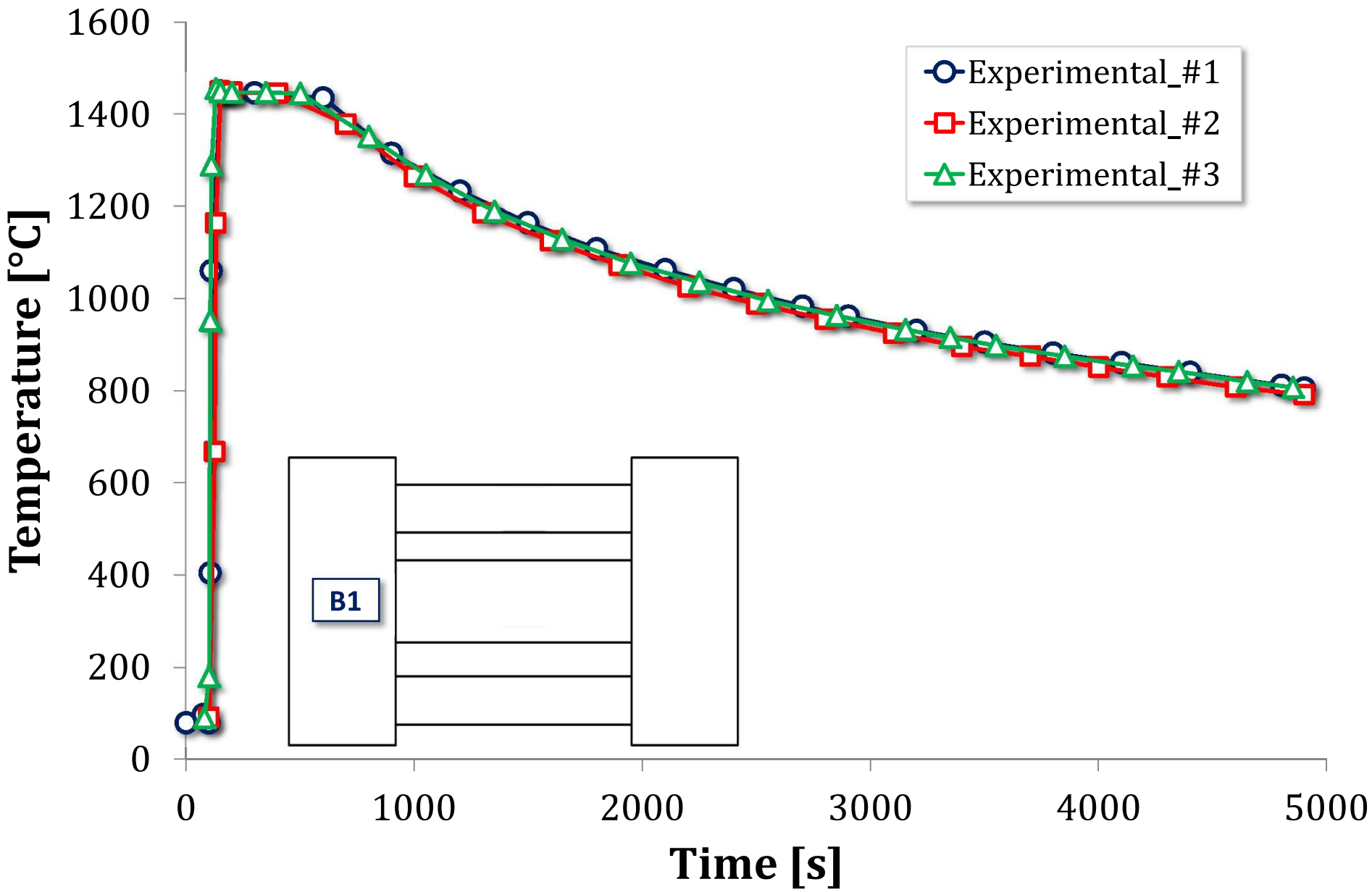
1600
1400
1200
1000
800
600
400
200
0
Temperature [°C]
0
1000
2000
3000
4000
5000
Time [s]
Experimental_#1
Experimental_#2
Experimental_#3
B1

Figure 10.

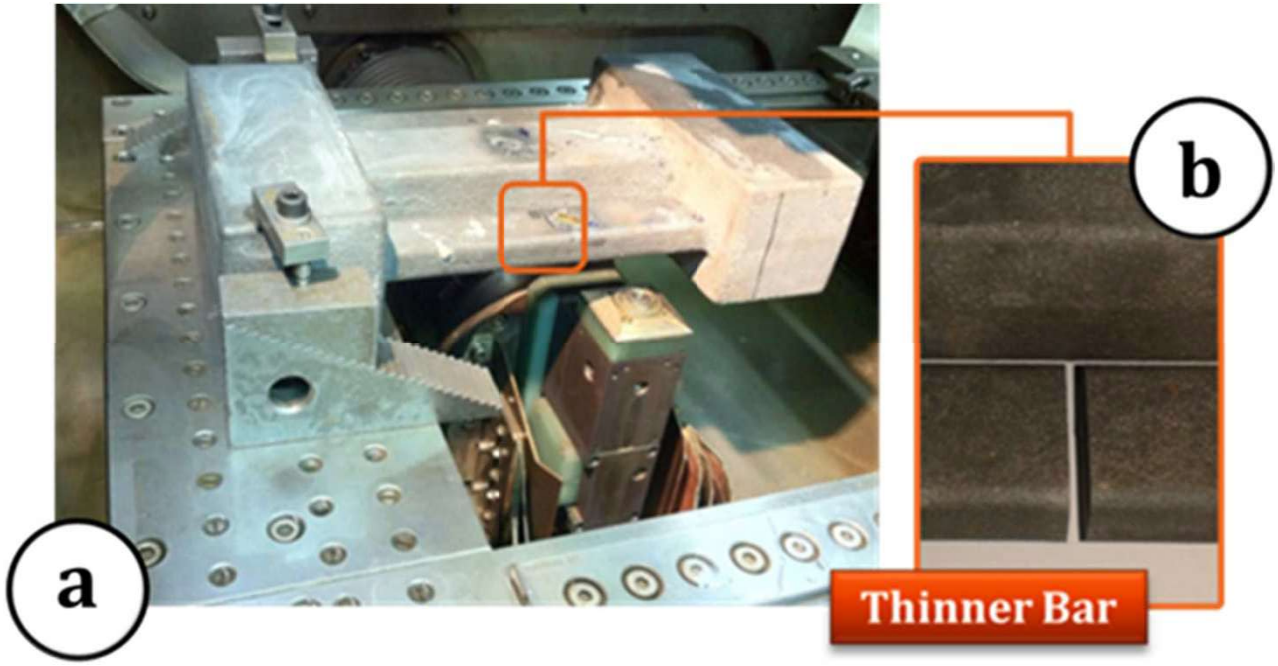

Figure 11a.

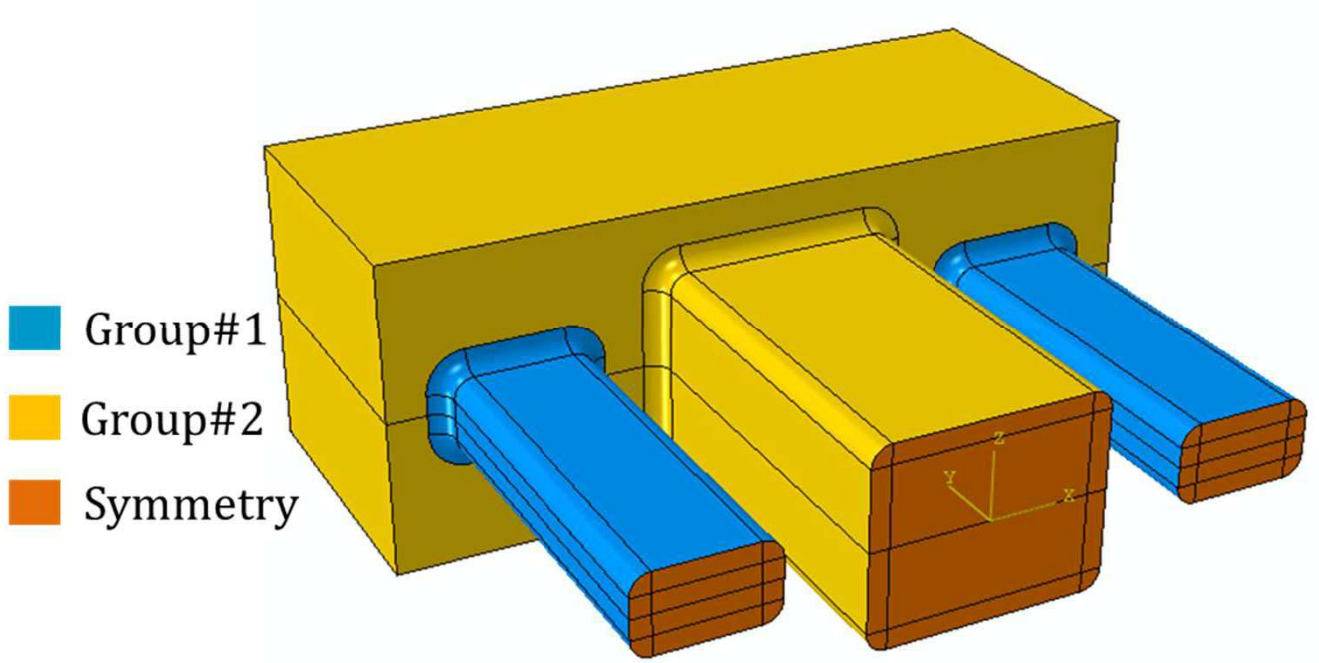

Figure 11b

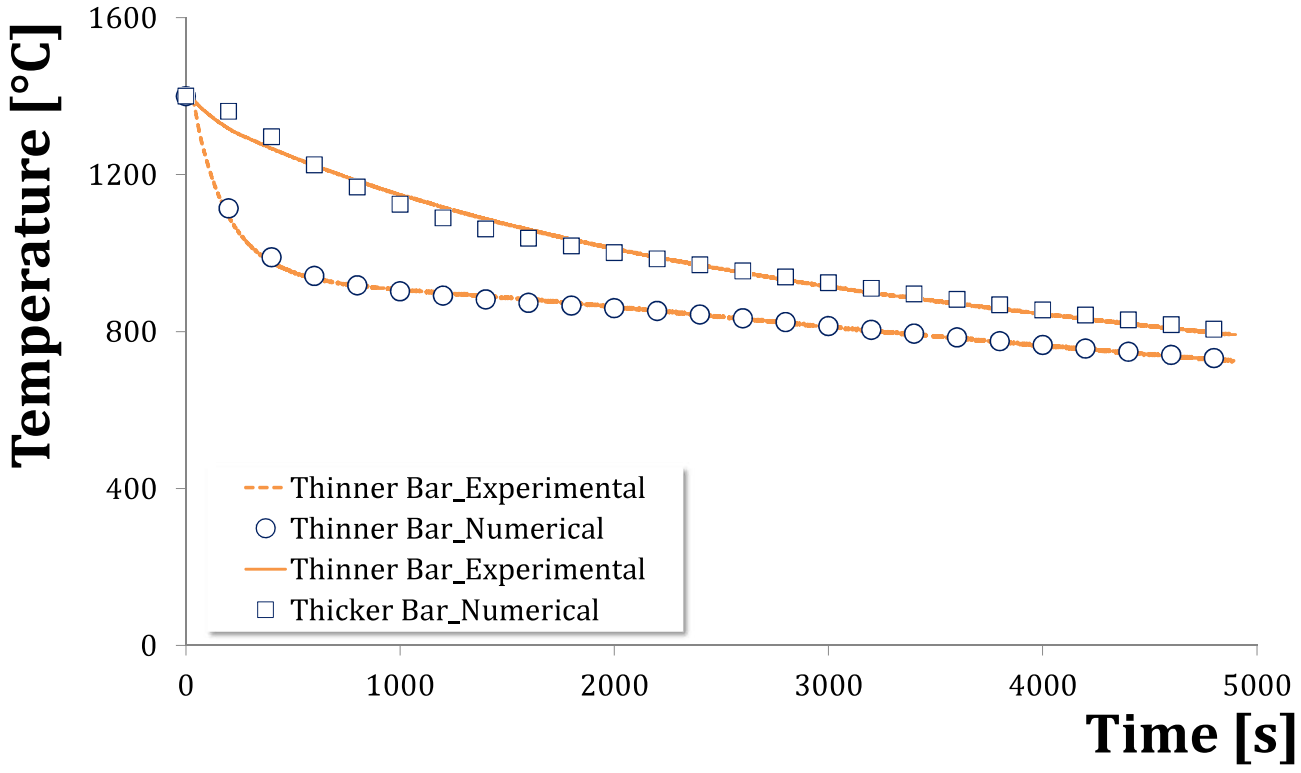
Temperature [°C]
1600
1200
800
400
0
0
1000
2000
3000
4000
5000
Time [s]
Thinner Bar_Experimental
Thinner Bar_Numerical
Thinner Bar_Experimental
Thicker Bar_Numerical

Figure 12a

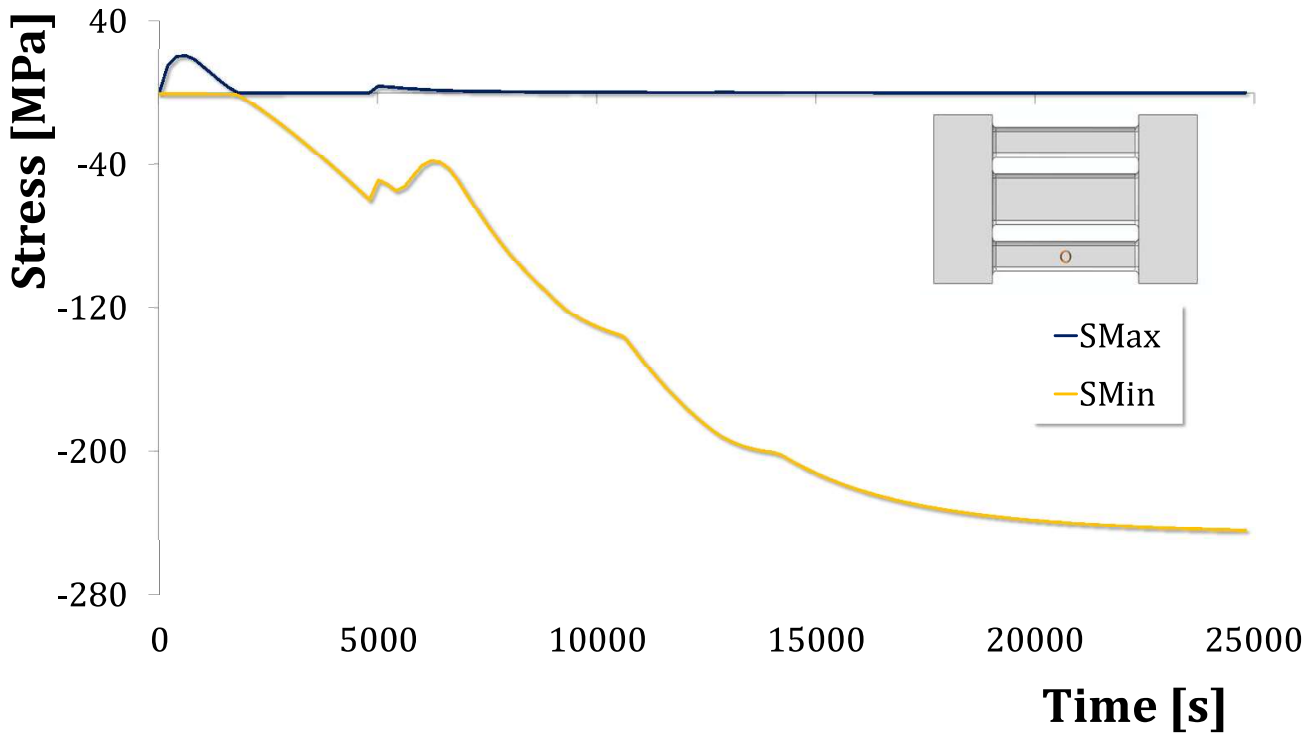
Stress [MPa]
40
-40
-120
-200
-280
0
5000
10000
15000
20000
25000
Time [s]
SMax
SMin

Figure 12b

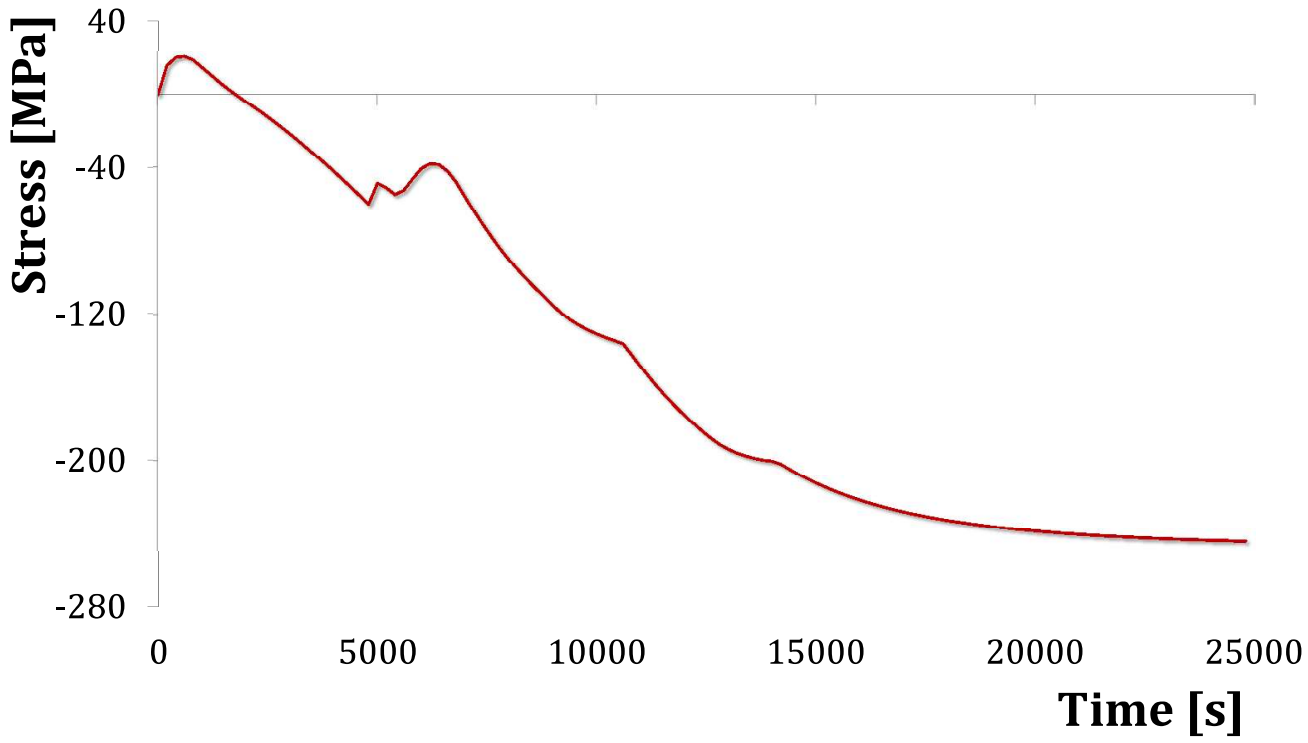
Stress [MPa]
40
-40
-120
-200
-280
0
5000
10000
15000
20000
25000
Time [s]

Figure 12c

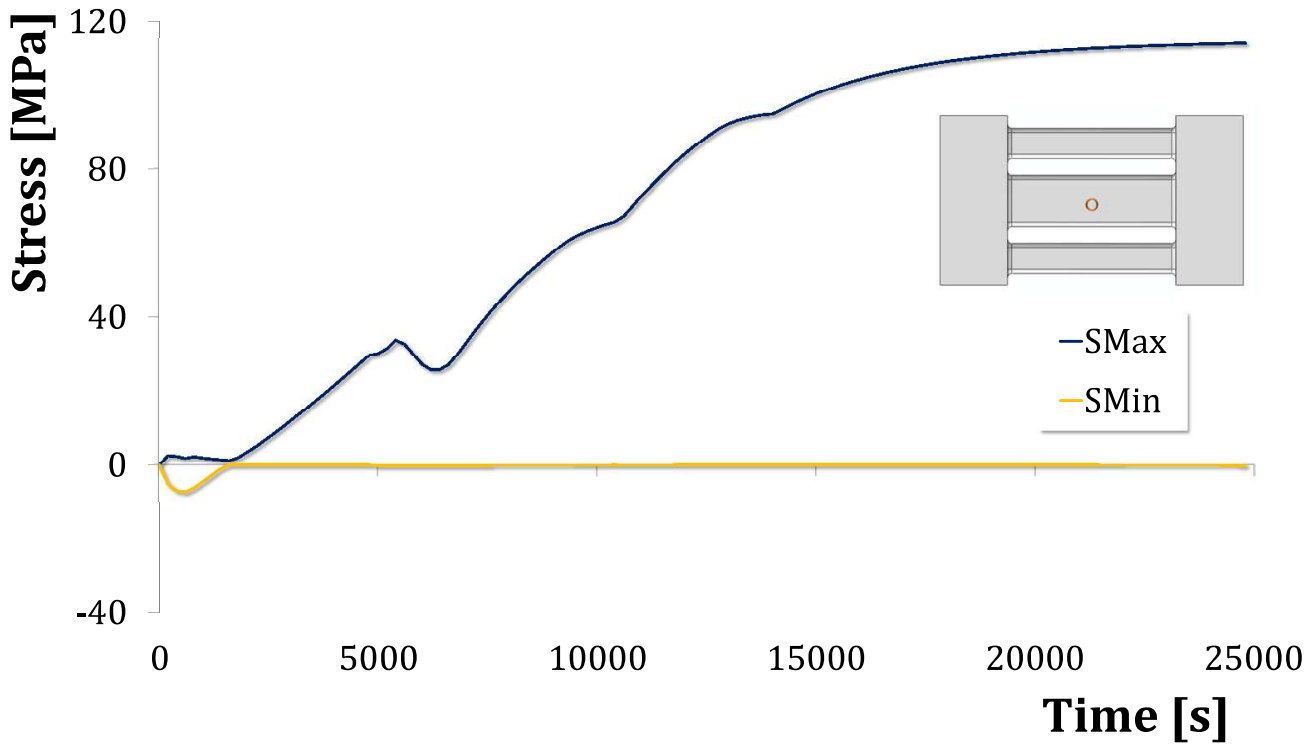
Stress [MPa]
120
80
40
0
-40
0
5000
10000
15000
20000
25000
Time [s]
SMax
SMin

Figure 12d

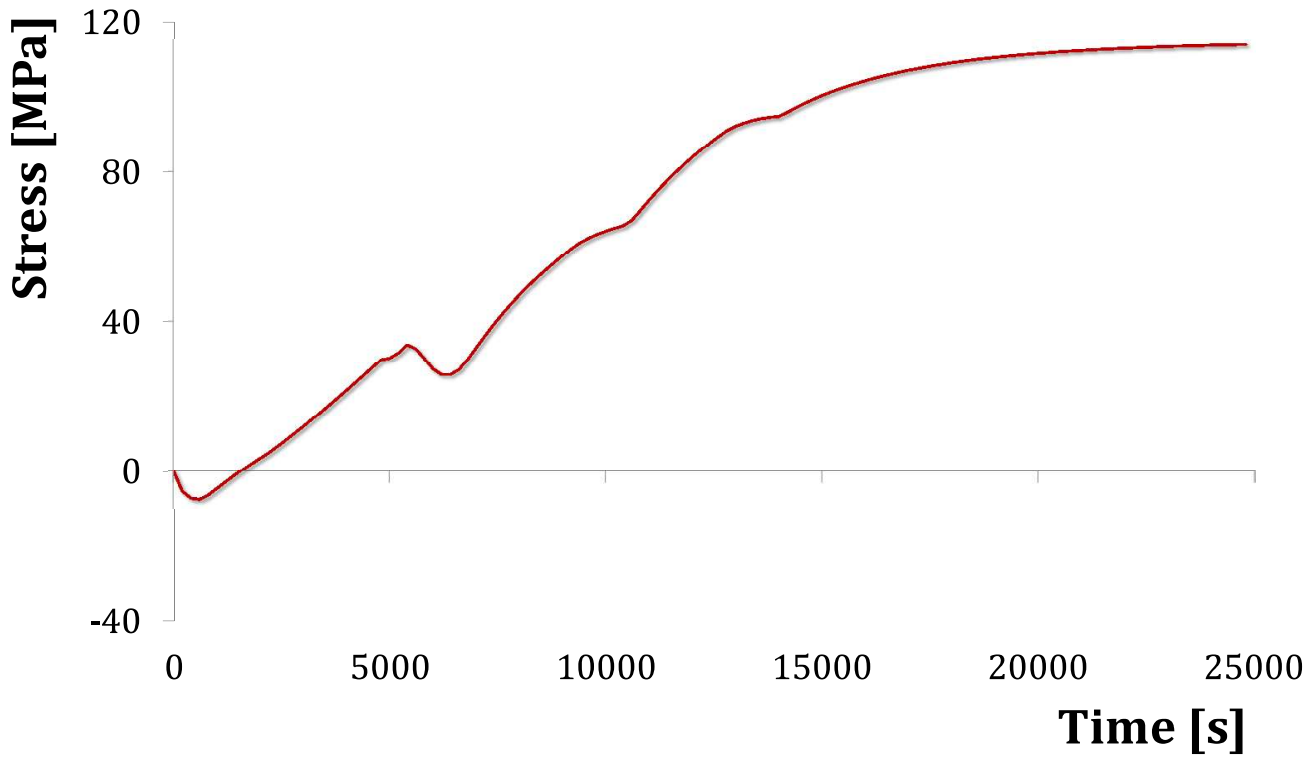

Figure 13a

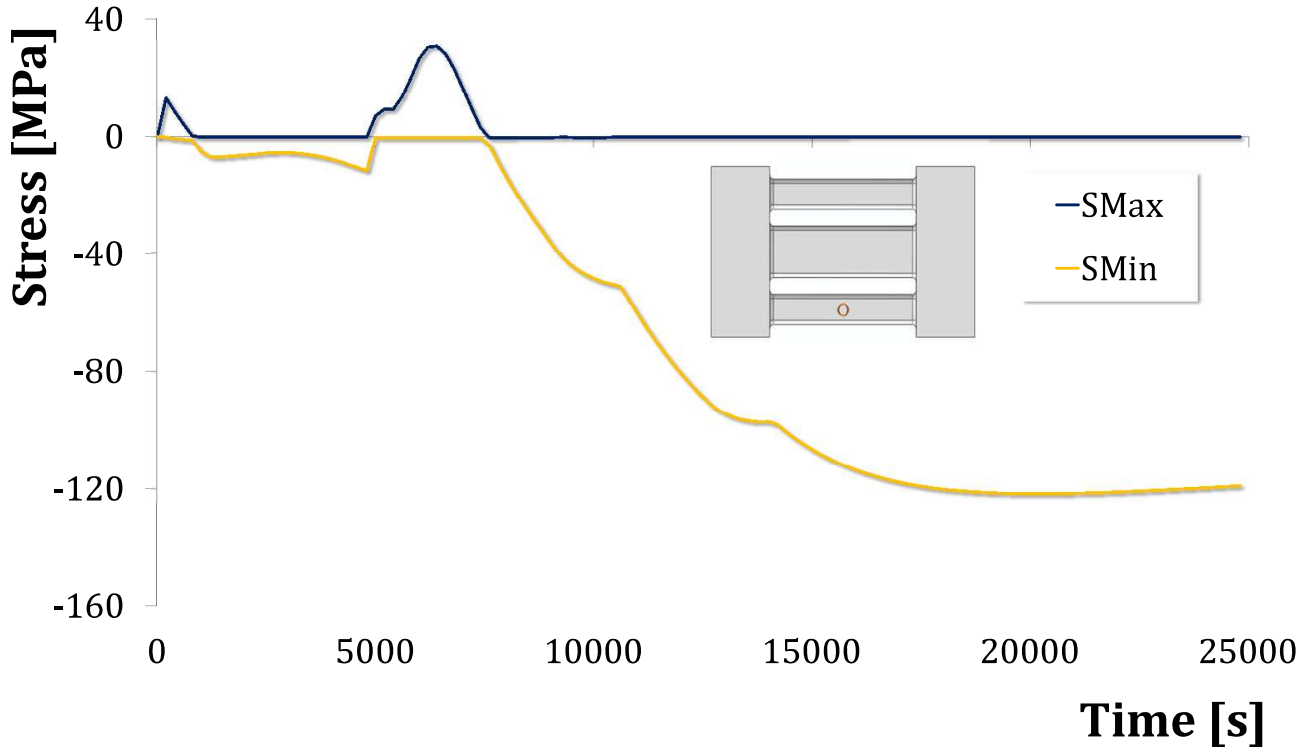
40
0
-40
-80
-120
-160
Stress [MPa]
0
5000
10000
15000
20000
25000
Time [s]
SMax
SMin

Figure 13b

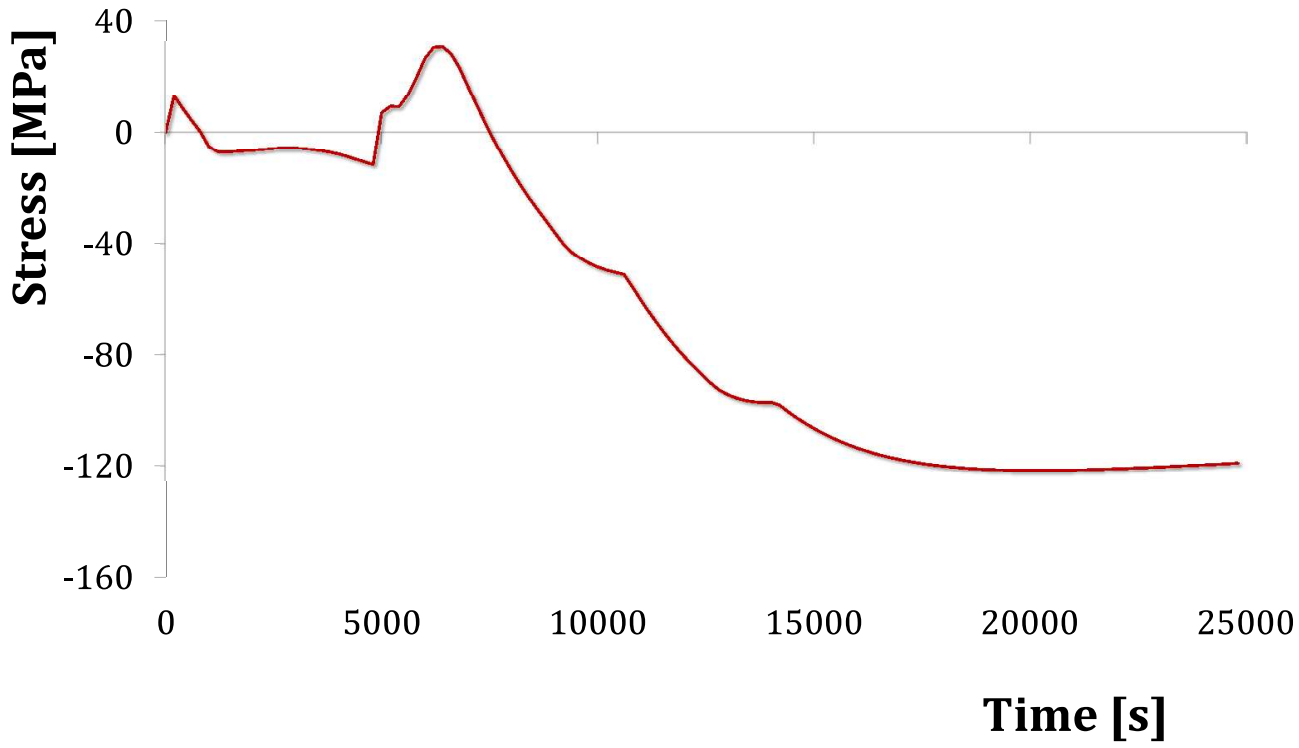
Stress [MPa]
40
0
-40
-80
-120
-160
0
5000
10000
15000
20000
25000
Time [s]

Figure 13c

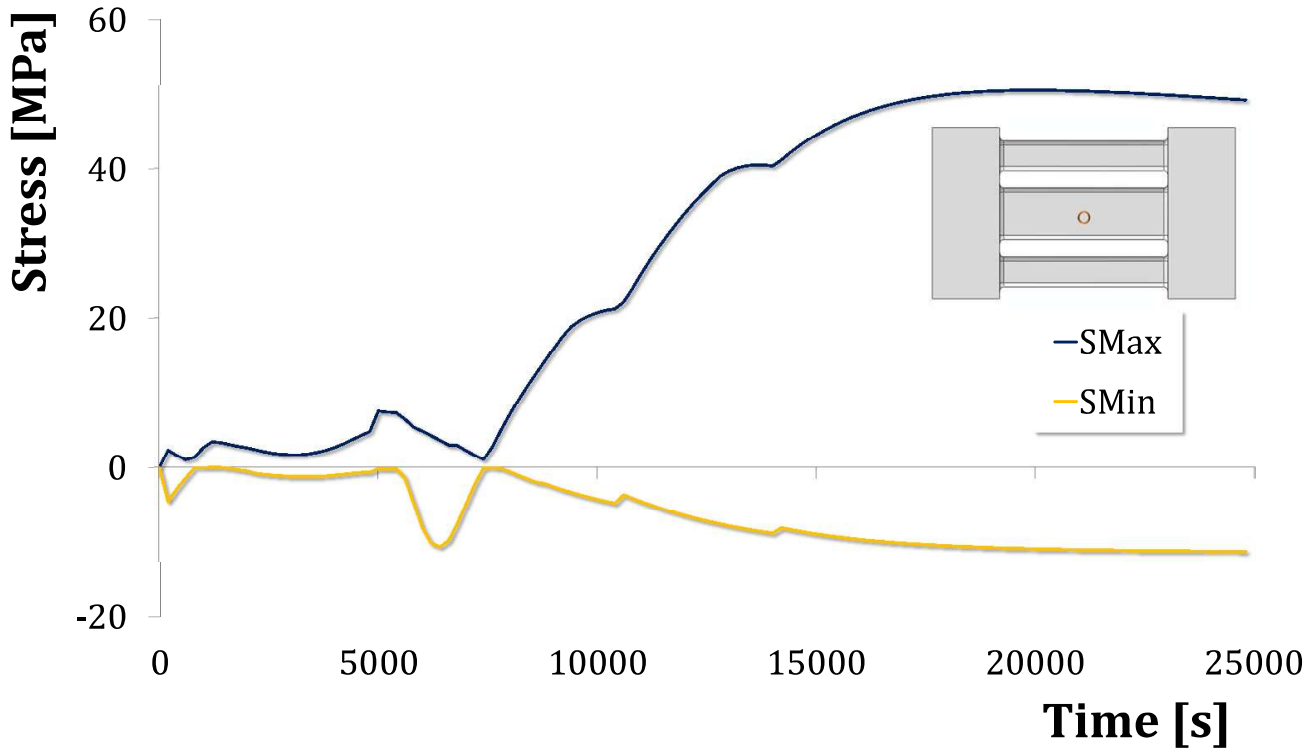
Stress [MPa]
60
40
20
0
-20
0
5000
10000
15000
20000
25000
Time [s]
SMax
SMin

Figure 13d

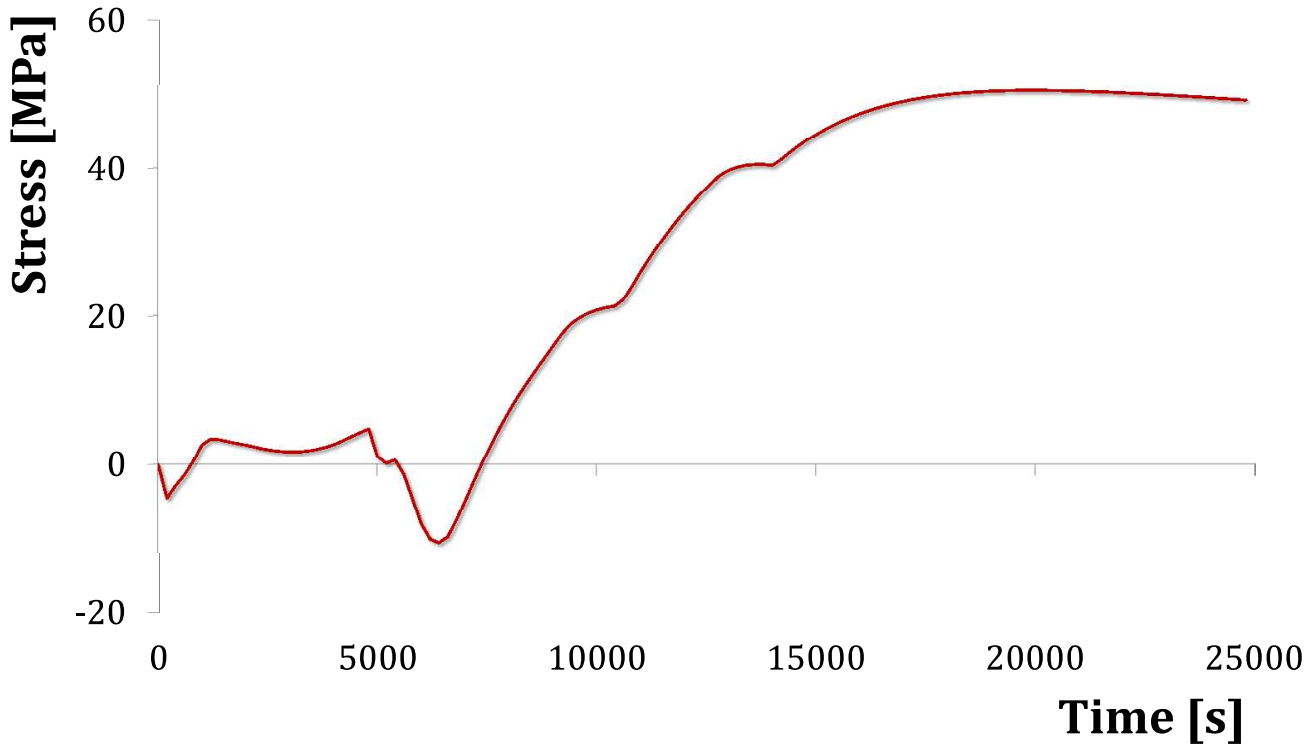

Figure 14a

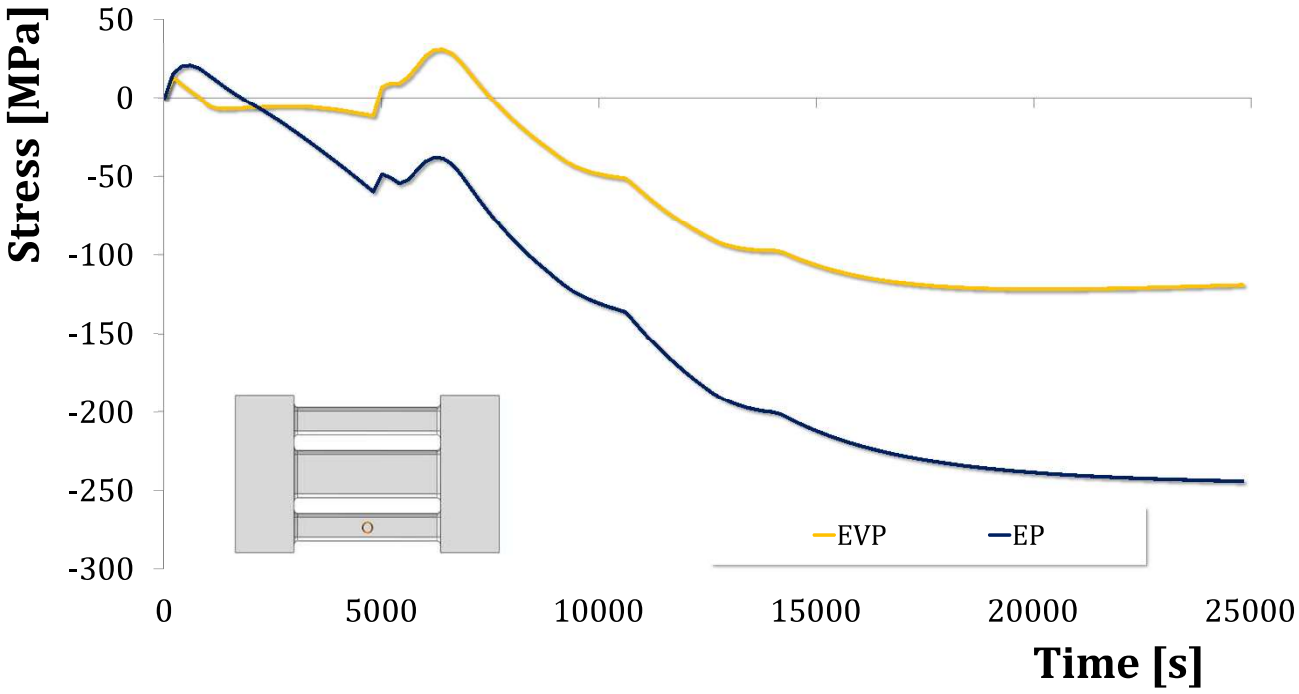
Stress [MPa]
50
0
-50
-100
-150
-200
-250
-300
0
5000
10000
15000
20000
25000
Time [s]
EVP
EP

Figure 14b

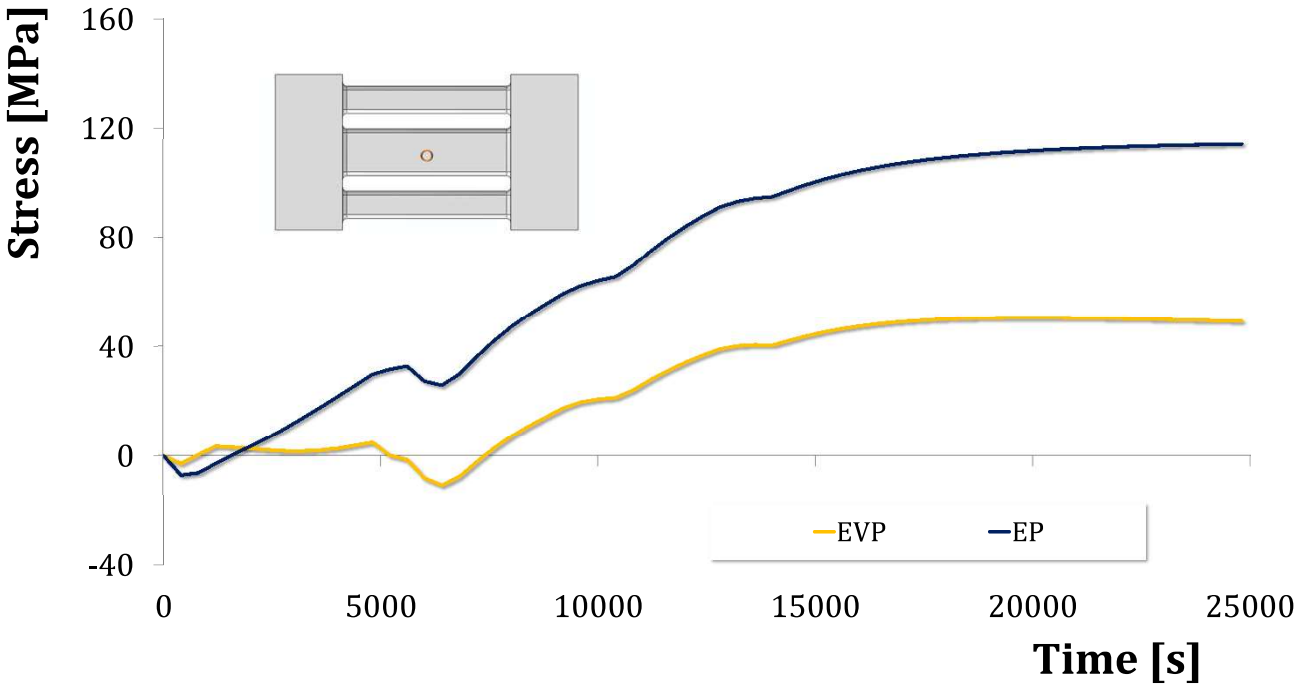
Stress [MPa]
160
120
80
40
0
-40
0
5000
10000
15000
20000
25000
Time [s]
EVP
EP

Figure 15.

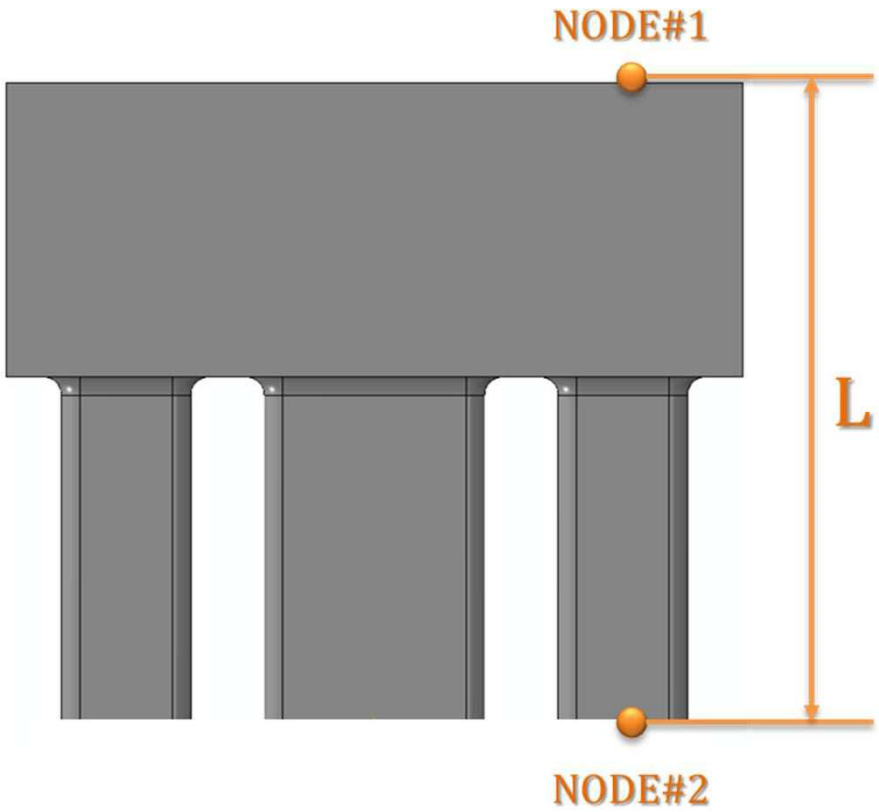

Table 1 Experimental casting: main quotes of the two considered geometries

Quotes Label	Geometry A [mm]	Geometry B [mm]
B	200	180
C	80	80
D	80	80
E	200	190
F	60	40
G	35	35
H	20	35
K	50	40

Table 2

Table 1. ASTM A890 Gr5A chemical composition

C %	Cr %	Ni %	Mo %	N %
<0.03	25.0	7	4.2	0.18

Table 3

Table 3. List of the obtained HTCs

Temperature [°C]	Group#1 HTC [W/m²K]	Group#2 HTC [W/m²K]
670	3.50E-05	3.00E-05
1000	1.00E-04	3.00E-05
1200	1.80E-04	7.00E-05
1300	1.80E-04	8.00E-05

Table 4

Table 4. Comparison of numerical and experimental displacement due to stress relaxation

	Geometry A Relaxation [mm]	Geometry B Relaxation [mm]
Experimental	0.065	0.01
Numerical (Elasto-Viscoplastic)	0.069	0.017
Numerical (Elasto-plastic)	0.143	0.029